



Crouch, E., Shepherd, C., Morgans, H., Naafs, B. D. A., Dallanave, E., Phillips, A., Hollis, C., & Pancost, R. D. (2020). Climatic and environmental changes across the Early Eocene Climatic Optimum at mid-Waipara River, Canterbury Basin, New Zealand. *Earth-Science Reviews*, 200, [102961].
<https://doi.org/10.1016/j.earscirev.2019.102961>

Peer reviewed version

License (if available):
CC BY-NC-ND

Link to published version (if available):
[10.1016/j.earscirev.2019.102961](https://doi.org/10.1016/j.earscirev.2019.102961)

[Link to publication record in Explore Bristol Research](#)
PDF-document

This is the author accepted manuscript (AAM). The final published version (version of record) is available online via Elsevier at <https://www.sciencedirect.com/science/article/pii/S0012825219302892>. Please refer to any applicable terms of use of the publisher.

University of Bristol - Explore Bristol Research

General rights

This document is made available in accordance with publisher policies. Please cite only the published version using the reference above. Full terms of use are available:
<http://www.bristol.ac.uk/red/research-policy/pure/user-guides/ebr-terms/>

**Climatic and environmental changes across the Early Eocene Climatic Optimum at mid-
Waipara River, Canterbury Basin, New Zealand**

E.M. Crouch¹, C.L. Shepherd¹, H.E.G. Morgans¹, B.D.A. Naafs², E. Dallanave³, A. Phillips¹, C.J.
Hollis¹, R.D. Pancost²

¹GNS Science, P.O. Box 30368, Lower Hutt, New Zealand

²Organic Geochemistry Unit, School of Chemistry, School of Earth Sciences, and Cabot Institute for
the Environment, University of Bristol, UK

³Research Group Marine Geophysics, Faculty of Geosciences, University of Bremen, GEO Gebäude,
Klagenfurter Straße, 28359 Bremen, Germany

Abstract

The Cretaceous–Paleogene marine sedimentary succession exposed in the banks of the middle reaches of the Waipara River (referred to as mid-Waipara), north Canterbury, New Zealand, has been the subject of several high-profile studies of Paleogene paleoclimate over the past decade. It is one of relatively few sections globally where a multi-proxy approach is possible due to the good preservation of microfossils and organic biomarkers. The Eocene section is also well dated by magnetostratigraphy and biostratigraphy based on planktic foraminifera, calcareous nannofossils and dinoflagellate cysts (dinocysts). Here, we build on this previous work and undertake a comprehensive analysis of paleontological and geochemical indicators of climatic and environmental changes through the early–middle Eocene part of the section, with particular focus on the Early Eocene Climatic Optimum (EECO; 53.26–49.14 Ma). We correlate a 33.5 m-thick interval with the EECO, based on biostratigraphy, magnetostratigraphy, TEX_{86} -paleothermometry and bulk carbonate $\delta^{13}\text{C}$. Our new sea-surface temperature (SST) record based on TEX_{86} agrees with a previous lower resolution record based on TEX_{86} and planktic foraminiferal $\delta^{18}\text{O}$ and Mg/Ca ratios. The EECO interval in this section extends from the upper part of the New Zealand Waipawan Stage to the Mangaorapan/Heretaungan Stage boundary at 49.27 Ma. The EECO onset is not exposed, but the termination is well constrained by a fall in SST and shift to more positive $\delta^{13}\text{C}$ values. Six negative carbon isotope excursions (CIEs) are recognised within the EECO and are tentatively correlated with CIEs J/K, M, O, Q, T and C22nH4 in the global $\delta^{13}\text{C}$ compilation. The CIEs are associated with warmer SSTs, indicating that they represent hyperthermals. The BAYSPAR TEX_{86} calibration indicates SST increased by as much as 12°C from the early Eocene (~55 Ma) to the EECO, where SST peaked at 35°C. SST gradually declined from mid EECO (~51 Ma) into the middle Eocene. The marked warming in the early EECO is associated with the highest abundance of warm-water taxa in calcareous nannofossil and dinocyst assemblages, the highest proportion of planktic foraminifera, and a coeval long-term shift to abundant angiosperm vegetation, primarily driven by a rise in Casuarinaceae. There is good agreement between TEX_{86} and marine microfossil-based proxies for temperature, providing confidence that both approaches are useful guides to past water temperature. Warm-water marine taxa are most abundant in

the EECO but are not dominant. Comparison of the abundance of nannofossil warm-water taxa between mid-Waipara and a low-latitude site on Shatsky Rise suggests the latitudinal temperature gradient between mid- and low-latitudes in the EECO was greater than the TEX₈₆ proxy implies. There is no clear evidence for enhanced sedimentation rates associated with the EECO, in contrast to evidence from the nearby Mead Stream section. Superabundant *Homotryblum*, a euryhaline dinocyst, in the early and middle EECO suggests elevated salinity and/or stratified surface waters, and there is no clear evidence of increased surface productivity associated with the EECO. Declining SST in the late EECO, ~50 Ma, corresponds with an increase in cool-water taxa and terrigenous material. This article highlights the importance of combining well-calibrated paleontological and geochemical records to better constrain and understand past warm climate states.

1. Introduction

A succession of short- and long-term global warming events during the early Eocene (56–48 Ma) provide important insights into climate variability under background conditions of elevated atmospheric CO₂, generally exceeding 800 ppmv (Zachos et al., 2008; Anagnostou et al., 2016; Hollis et al., 2019). Well-calibrated sedimentary records for this time period from different regions are essential to understand the geographic variability in climate and ecosystem response and to validate Earth system models (Huber and Cabellero, 2011; Lunt et al., 2017). Records from the South Pacific are of particular interest because the Pacific Ocean was the primary driver of ocean heat transport during the Paleogene (Huber and Nof, 2006). Both model and proxy studies indicate that the Pacific sector of the Southern Ocean was a major source of deep water through most of the Paleogene (Littler et al., 2014; Huck et al., 2017). For this reason, the Southwest Pacific has been the focus of several studies of early Paleogene climate dynamics over the past two decades (e.g., Crouch et al. 2003; Nicolo et al., 2007; Bijl et al., 2009, 2013a; Hollis et al., 2009, 2012, 2015; Slotnick et al., 2012, 2015; Pancost et al., 2013; Taylor et al., 2013; Dallanave et al., 2014, 2016; Inglis et al., 2015; Hines et al., 2017; Naafs et al., 2018).

The lower Paleogene succession at mid-Waipara River, Canterbury Basin, New Zealand (Fig. 1), has been a focus of many of these studies because the siliciclastic sediments contain a wide range of microfossils as well as immature organic matter suitable for biomarker studies. Studies have investigated both marine and terrestrial temperature records from latest Cretaceous to middle Eocene, focusing on glycerol dialkyl glycerol tetraethers (GDGTs; Hollis et al., 2009, 2012, 2014; Pancost et al., 2013; Taylor et al., 2013, 2018) as well as Mg/Ca ratios and oxygen isotopes (Hollis et al. 2009, 2012; Creech et al. 2010; Hines et al., 2017). These studies have provided multiproxy estimates of temperature, which have been compared with climate and general circulation models (Huber and Caballero, 2011; Hollis et al., 2012; Lunt et al., 2012). The Eocene section also has a well-calibrated age model that incorporates dinocyst, foraminiferal and nannofossil biostratigraphy and magnetostratigraphy (Dallanave et al. 2016; Shepherd and Kulhanek, 2016). Whilst paleontology has supported these studies, the focus has been on biostratigraphy rather than paleontological indicators of

climatic and environmental change in the Eocene greenhouse world. In this article, we utilise the well-preserved calcareous and organic-walled microfossil assemblages in this continental margin section to evaluate proxy- and model-based climate reconstructions and to infer the biological response to changes in climate and carbon cycling.

Our multidisciplinary study includes analysis of foraminiferal, calcareous nannofossil, dinoflagellate cyst (dinocyst) and spore/pollen assemblages, bulk carbonate $\delta^{13}\text{C}$ isotopes, CaCO_3 content, and biomarkers (GDGTs), and utilises samples collected as part of our magnetostratigraphic study (Dallanave et al., 2016) of the lower and middle Eocene succession at mid-Waipara River. We document the timing and variability of environmental and climatic changes in the marine and terrestrial realm, and compare these changes with a new and more detailed record of sea surface temperature (SST) and carbon cycle change than has been previously reported for this section.

2. Identifying the Early Eocene Climatic Optimum (EECO)

The warmest sustained temperatures of the Cenozoic occurred in the EECO (Zachos et al., 2001, 2008; Westerhold and Röhl, 2009; Laetano et al., 2016; Evans et al., 2018) and were associated with atmospheric CO_2 levels of >800 ppmv (Beerling and Royer, 2011; Anagnostou et al., 2016; Boudreau et al., 2019; Hollis et al., 2019). The EECO (Fig. 2) was initially defined by a minimum in oxygen isotope ($\delta^{18}\text{O}$) values of benthic foraminifera that lasted 2–3 Myrs, from ~53–50 Ma (Zachos et al., 2001; Kirtland Turner, 2014). Recent studies indicate that the EECO onset can be tied to one of several carbon isotope excursions (CIEs) from the middle early Eocene (Cramer et al., 2003; Westerhold et al., 2012; Laetano et al., 2015, 2018). A new astronomically-tuned, benthic foraminiferal record at ODP Site 1209, North Pacific, recommends that the J event, dated at 53.26 Ma, be adopted as the base of the EECO (Westerhold et al., 2018). In the hemipelagic succession of eastern Marlborough, New Zealand (Fig. 1), this CIE coincides with a transition from limestone to marl-dominated sediments (Hollis et al., 2005 a, b), which is inferred to reflect hydrological changes linked to the EECO (Slotnick et al., 2012, 2015; Dallanave et al., 2014). The top of the EECO is tied to

a CIE in uppermost Chron C22n (C22nH5), dated at 49.14 Ma, that is coincident with the onset of a long-term cooling trend in the benthic $\delta^{18}\text{O}$ record (Westerhold et al., 2018).

Thus, the EECO is currently considered to extend from 53.26 Ma to 49.14 Ma, Chron C24n.2rH1 (J event) to uppermost Chron C22n (CIE C22nH5), an interval of 4.12 Myrs that extends from the upper part of calcareous nannofossil zone NP11 to lower NP14 (Hollis et al., 2019). In terms of New Zealand stages (Raine et al., 2015), the EECO extends from the late Waipawan to close to the Mangaorapan/Heretaungan boundary (49.27 Ma) and includes the Waipawan/Mangaorapan boundary at 52 Ma (Fig 2).

3. Previous early to middle Eocene studies at mid-Waipara River

The lower–middle Eocene Ashley Mudstone succession outcrops along the river bed (Fig. 1), and three sample suites have been collected (Supp. Information Fig. 1). Two suites, from 2003 and 2007, are integrated into one composite section (Morgans et al., 2005) and have been the focus of several studies, including $\delta^{13}\text{C}$ isotopes, Mg/Ca ratios, GDGT analyses, and biostratigraphy (Hollis et al., 2009, 2012; Creech et al., 2010; Pancost et al., 2013; Taylor et al., 2013; Inglis et al., 2015). As part of a magnetostratigraphic study (Dallanave et al., 2016), a third suite was taken in 2012 (Fig. 3) from the same river bed section as the 2003 collection. Oriented samples for paleomagnetic analyses were taken over a ~45 m stratigraphic interval. Six magnetic polarity reversals were correlated to magnetic polarity Chrons C23n.2n to C21 n, with the aid of nannofossil and foraminiferal biostratigraphy. This correlation spans from ~51.5–47 Ma, based on the orbitally-tuned Eocene timescale of Westerhold et al. (2017), and provides a magnetostratigraphically calibrated age for the base of the NZ Heretaungan Stage, i.e., 49.27 Ma (C22n(0.6)).

Following the recommendation of van Hinsbergen et al. (2015), our paleogeographic reconstruction (Fig. 1) and Eocene locations of the sites mentioned in the text are based on a paleomagnetic reference frame (Matthews et al., 2016). This reference frame is more suitable than a mantle-based reference frame for paleoceanographic and paleoclimate studies because it is tied to the

Earth's spin axis and therefore more accurately represents true paleolatitude. As noted by van Hinsbergen et al. (2015), this change in reference frame moves Southwest Pacific Paleogene sites northward by $\sim 10^\circ$ and the mid-Waipara site shifts from the previously reported paleolatitude of 55°S (e.g. Hollis et al., 2009, 2012) to 46°S (Fig. 1).

4. Material and methods

4.1 Mid-Waipara River section and samples

The mid-Waipara River section (Fig. 1) is situated ~ 13 km west of the Waipara township, north Canterbury, and includes the area downstream from Doctors Gorge to top of the Amuri Limestone in what is referred to as the 'lower gorge' (NZ Map Series 260, reference M34/755 946–M34/789 944). The Ashley Mudstone comprises low-dipping calcareous mudstone outcropping in the river bed (Morgans et al., 2005). Strata are well-exposed in the central part, but exposure is more variable in the upper and lower parts, and highly dependent on river level and sediment load. Samples are examined from two suites, the 2007 and 2012 collections (Fig. 3; Supp. Information Fig. 1). The two collections are correlated by biostratigraphy and lithology, as the reference marker used in the 2007 collection was washed away and direct field correlation was not possible. The base of the 2012 (M34/f930) and top of the 2007 (M34/f889) collections are inferred to be separated by a stratigraphic gap of ~ 1 m. Eleven samples (M34/f899–f889) were collected in 2007 from ~ 15 m of stratigraphic section, although the middle part of the section (-13.2 to -6.6 m) could not be sampled as the river level was too high. In 2012, a detailed suite of 118 samples (M34/f930–f1047) were taken from ~ 66.5 m of section.

4.2 Microfossils

Biostratigraphic and paleoenvironmental studies were completed for foraminifera, calcareous nannofossils, dinocysts, and spores and pollen. All paleontological samples, residues and slides are

stored in the National Paleontological Collection at GNS Science, Lower Hutt, NZ. Biostratigraphic data are in the Appendix (Supp. Information).

4.2.1 Foraminifera

A total of 92 samples were processed, with 500 g of dried sediment washed over a 75 µm screen for each sample. The residues were then dried, reweighed and half was retained for a quantitative census. The remaining half of the residues were qualitatively picked to obtain a comprehensive faunal assemblage that was used for biostratigraphy and paleodepth. A subsequent count was completed to calculate the planktic/benthic foraminiferal ratio, and this value is expressed as the proportion of planktic specimens in the total foraminiferal assemblage (planktic abundance).

4.2.2 Calcareous nannofossils

Smear slides were made for 34 samples using standard techniques (Bown and Young, 1998). In some cases, samples contained a large amount of fine sand and strewn slides were prepared according to the method of Bown and Young (1998). Slides were analysed using an Olympus BX53 microscope at 1000x magnification in plane-transmitted light (PL), cross-polarized light (XPL) and phase contrast (PC) light. Relative abundance of taxa was determined from counts of 450 specimens along random traverses of each slide, followed by scanning to identify additional rare species. Specimens were identified to species level following the taxonomic concepts of Perch-Nielsen (1985), Bown (1998, 2005), Dunkley Jones et al. (2009) and Shamrock and Watkins (2012). Results are correlated to the zonation scheme of Martini (1971), with subzones as defined by Aubry (1991) and absolute ages for events calibrated to Gradstein et al. (2012) and Hollis et al. (2019). Full synonymies for all taxa mentioned in this paper are available in the publications listed above. To examine paleotemperature changes, we distinguish cool- and warm-water taxa based on previous studies that use statistical analyses of assemblage data (e.g., cluster analysis, principal component analysis) to interpret patterns and relationships among taxa (e.g. Wei and Wise, 1990; Siesser, 1993; Bralower,

2002; Villa and Persico, 2006; Villa et al., 2008; Schneider et al., 2011; Shamrock and Watkins, 2012). Cool-water taxa comprise *Chiasmolithus* spp. and *Reticulofenestra daviesii*, while warm-water taxa comprise *Discoaster* spp., *Sphenolithus* spp. and *Coccolithus formosus*.

4.2.3. Palynomorphs

A total of 45 samples were processed using standard palynological processing techniques. Between 21 and 31 g of sediment was crushed, dried and the carbonate and siliceous component removed by adding 10% HCl and 50% HF, respectively. Samples were oxidised, for up to 10 minutes, using 70% HNO₃ and washed with 5% NH₄OH to disaggregate amorphous and organic debris. Some samples were placed in an ultrasonic bath (for up to 1 minute) prior to sieving. All samples were sieved over a 6 µm mesh, and well-mixed representative fractions of the >6 µm residue mounted on glass slides using a glycerine jelly medium. The relative abundance of palynomorphs was determined in three ways; 1) ~200 dinocysts counted for 43 samples, 2) ~200 spores/pollen counted for 33 samples, and 3) ~150 marine and terrestrial palynomorphs counted for 37 samples. At least one extra slide was scanned for additional rare species. Quantitative results are shown as a percentage of the total count, or with reference to the following: rare (1–5%), common (6–10%), frequent (11–20%), abundant (21–40%) and super abundant (>40%). Dinocyst biostratigraphy is correlated to the established New Zealand zonation (Morgans et al., 2004), with early Eocene zones based on Crouch (2001; Fig. 2). An alternative South Pacific zonation (Bijl et al., 2013a) is not utilised because several index species are either not present at mid-Waipara (e.g., lowest occurrence (LO) of *Arachnodinium antarcticum*) or seem to have diachronous ranges (e.g. highest occurrence (HO) of *Palaeocystodinium golzowense* is older in New Zealand than recorded at ODP Site 1172, East Tasman Plateau).

To examine paleotemperature changes, we distinguish taxa with a low-latitude (warm-water) affinity from those with a Southern Ocean (cooler-water) affinity. Our warm-water group includes taxa of the Wetzelielloideae subfamily: *Apectodinium*, *Charelsdowniea*, *Dracodinium*, *Rhombodinium*, *Wetzeliella* and *Wilsonidium*. The genus *Apectodinium* evolved in equatorial regions, with a LO close to the Danian/Selandian boundary (~61 Ma, Guasti et al., 2005; Awad and Oboh-

Ikuenobe, 2016), while other Wetzelielloideae taxa (*Rhombodinium*, *Wilsonidium*) have LOs in north-east India (Prasad et al., 2006) and the Tethys (Iakovleva and Heilmann-Clausen, 2007) in sediments dated as latest Paleocene. Recent work suggests the lower SST tolerance of Wetzelielloideae was $20 \pm 2.5^{\circ}\text{C}$ (Frieling et al., 2014). The genus *Homotryblum* also evolved in low latitudes, with a LO near the base of the Thanetian (upper Foraminifera Zone P4a, Iakovleva et al., 2001; Crouch et al., 2003; Slimani et al., 2016). We keep the *Homotryblum* genus separate from the Wetzelielloideae group as it has a different morphology and may have had a broader SST range, from tropical–warm temperate (Köthe, 1990; Brinkhuis, 1994), although a recent study suggests it is part of an epicystal Goniodomideae ecogroup that preferred SSTs $>25 \pm 2.5^{\circ}\text{C}$ (Frieling and Sluijs, 2018). Taxa associated with the Endemic Antarctic Community (EAC), or transantarctic community (Wrenn and Beckman, 1982; Bijl et al., 2011), are found south of $\sim 45^{\circ}\text{S}$ (Bijl et al., 2013b) and may have preferred cooler Antarctica-derived surface currents, particularly in the late early Eocene–late Eocene (Bijl et al., 2011, 2013b). In this study we identify a limited number of EAC taxa, comprising *Alterbidinium assymmetricum*, *Deflandrea antarctica*, *Enneadocysta* group and *Spinidinium macmurdoense*. Whilst Bijl et al. (2013b) considered *Membranophoridium perforatum* to be part of the EAC, we do not include this taxon as it appears to have extended north of 45°S in some regions (Wilson, 1988).

4.3 Stable isotopes and carbonate content

A total of 68 samples were analysed for carbonate content and bulk carbonate $\delta^{13}\text{C}$ and $\delta^{18}\text{O}$ at the National Isotope Centre, GNS Science. Samples were analysed on the GVI IsoPrime Preparation System at a reaction temperature of 25°C for 24 hours and run via dual inlet on the IsoPrime mass spectrometer. All results are reported with respect to VPDB, normalised to an internal GNS Marble standard (2.04‰ for $\delta^{13}\text{C}$ and -6.40‰ for $\delta^{18}\text{O}$). Precision is 0.1‰ for $\delta^{13}\text{C}$ and 0.2‰ for $\delta^{18}\text{O}$ (Appendix, Supp. Information).

4.4 Organic geochemistry

A total of 68 samples were analysed for glycerol dialkyl glycerol tetraethers (GDGTs) at the Organic Geochemistry Unit, University of Bristol (Appendix, Supp. Information). Sediments were freeze-dried and powdered with a pestle and mortar. Biomarker lipids were extracted from between 30 and 50 g of sediment using Soxhlet technique and 220 ml of a 9:1 mixture (v/v) of dichloromethane (DCM) and methanol (MeOH). Sediments were extracted for 24 hrs at ~70 °C with activated copper to remove elemental sulfur. The total lipid extract (TLE) was concentrated using a rotary evaporator, then dried under a gentle flow of nitrogen. Open column flash chromatography (alumina) was used to separate the TLE into apolar and polar fractions using 4 ml of dichloromethane (DCM):hexane (9:1) and 4 ml of DCM:Methanol (MeOH) (1:2), respectively. Both fractions were fully dried under a gentle flow of nitrogen. The polar fraction was redissolved in a mixture of hexane and *iso*-propanol (IPA) (99:1) and filtered through a 0.45 µm PTFE filter. Filtered polar fractions were analysed for their core-lipid GDGTs distribution by high performance liquid chromatography/atmospheric pressure chemical ionisation-mass spectrometry (HPLC/APCI-MS) using a ThermoFisher Scientific Accela Quantum Access triplequadrupole MS. Normal phase separation was achieved using two ultra-high performance liquid chromatography silica columns, following the methods of Hopmans et al. (2016). Injection volume was 15 out of 100 µl. Analyses were performed using selective ion monitoring mode (SIM) to increase sensitivity and reproducibility (*m/z* 1302, 1300, 1298, 1296, 1294, 1292, 1050, 1048, 1046, 1036, 1034, 1032, 1022, 1020, 1018, 744, and 653). Sample results were integrated manually using the Xcalibur software.

4.5 GDGT-based calibrations and indices

We used the distribution of isoprenoidal GDGTs as reflected in the TetraEther index of tetraethers consisting of 86 carbon atoms (TEX₈₆) to reconstruct SST (Schouten et al., 2002).

$$\text{eq. (1) } \text{TEX}_{86} = \frac{[\textit{isoGDGT-2}] + [\textit{isoGDGT-3}] + [\textit{cre. regio isomer}]}{[\textit{isoGDGT-1}] + [\textit{isoGDGT-2}] + [\textit{isoGDGT-3}] + [\textit{cren. regio isomer}]}$$

To capture the range of potential SST estimates that may be derived from this proxy we applied two different calibrations: the BAYSPAR deep time analogue calibration (Tierney and Tingley, 2014, 2015; Tierney et al., 2017), which is based on a linear relationship between TEX₈₆ and SST, and the TEX₈₆^H calibration (Kim et al., 2010), which is based on an exponential relationship (Hollis et al., 2019). The TEX₈₆^L calibration is not used because it has been found to have significant shortcomings (Hollis et al., 2019). The BAYSPAR deep-time calibration has been applied to reconstruct SSTs during greenhouse periods such as the early Paleogene (Naafs et al., 2018), PETM (Tierney and Tingley, 2014) and Cretaceous (Naafs and Pancost, 2016; O'Brien et al., 2017). For the BAYSPAR calibration, we used a prior of 30 ± 20°C and search tolerance of 0.13. The resulting analogue locations are all located in the tropics or subtropics, including the Red Sea (this data is excluded from the TEX₈₆^H calibration). Selecting different values for the prior (e.g. 25–35°C) does not result in significantly different SST results. Although part of our data lies above the modern calibration range for TEX₈₆, the data lie within the range of mesocosm experiments that indicate TEX₈₆ remains (linearly) correlated to temperature at SSTs up to 40 °C (Schouten et al., 2007). The BAYSPAR deep-time calibration incorporates this range into its error calculation.

Following Inglis et al. (2015) we identify an *iso*GDGT distribution similar to that found at present in the Red Sea (Trommer et al., 2009) using;

$$\text{eq. (2) } \text{isoGDGT}_{\text{rs}}(\%) = \frac{[\text{cren. regio isomer}]}{[\text{cren. regio isomer}] + [\text{isoGDGT-0}]} \times 100$$

In addition, we also calculate the Branched versus Isoprenoidal Tetraether (BIT) index (Hopmans et al., 2004).

$$\text{eq. (3) } \text{BIT} = \frac{Ia + IIa + IIa' + IIIa + IIIa'}{Ia + IIa + IIa' + IIIa + IIIa' + \text{cren.}}$$

BIT reflects the relative abundance of *br*GDGTs that are abundant in mineral soil and peat (Weijers et al., 2006; Weijers et al., 2007; Naafs et al., 2017b) versus a specific archaeal *iso*GDGT, crenarchaeol, produced by *Thaumarchaeota* that is more abundant in the marine realm (Sinninghe Damsté et al., 2002). High BIT values are typically found in soils and lacustrine archives, and are therefore

generally used to indicate a high input of terrestrial-derived GDGTs, which can result in unreliable SST estimates (Hopmans et al., 2004). However, it is important to note that brGDGTs can also be produced *in situ* in marine sediments and do not always purely reflect changes in terrestrial input (Sinninghe Damsté, 2016). BIT values <0.3 indicate terrestrial-derived GDGTs likely have little effect on TEX₈₆-based SST estimates (Hopmans et al., 2004).

The methane index (MI) (Zhang et al., 2011) is defined as;

$$\text{eq. (4) MI} = \frac{[\text{isoGDGT-1}] + [\text{isoGDGT-2}] + [\text{isoGDGT-3}]}{[\text{isoGDGT-1}] + [\text{isoGDGT-2}] + [\text{isoGDGT-3}] + [\text{Cren.}] + [\text{cren. regio isomer}]}$$

A MI >0.5 indicates a contribution of methanogens to the GDGT pool that can bias TEX₈₆-based SST.

5. Results

5.1 Stratigraphy, age control and fossil assemblages

The stratigraphy of the section is described in relation to five Eocene New Zealand Stages (Fig. 2): Waipawan, Mangaorapan, Heretaungan, Porangan and Bortonian (Cooper et al., 2004; Raine et al., 2015), which extend from earliest Eocene to latest middle Eocene (56 to 39.1 Ma).

Biostratigraphic data are in the Appendix (Supp. Information).

5.1.1. Lithostratigraphy

The ~80 m section is mainly a moderately indurated, partly calcareous, grey mudstone, which is glauconite rich in the upper part of the section. An abrupt coarsening of sediment occurs at ~59 m, with overlying sediments containing common medium- to coarse-grained glauconite (Fig. 3).

Magnetostratigraphy and calcareous microfossil biostratigraphy provide a good age framework (Dallanave et al., 2016). The section extends from lower–middle Eocene (~55.5–42 Ma; Waipawan–lower Bortonian), with an unexposed interval in the Waipawan part of the section (-13.1 to -6.7 m).

The abrupt change in sediment type at 59 m coincides with an unconformity that spans ~3 Myr:

uppermost Heretaungan, Porangan and lowermost Bortonian (middle Eocene) sediments are not preserved.

5.1.2 Foraminifera

Foraminifera are poorly preserved in the lowermost part of the section (-16.15 to -13.2 m), but an earliest Eocene (Waipawan) age is inferred from identifiable specimens of *Globanomalina australiformis* and *Morozovella aequa* (Fig. 3). Foraminifera are relatively well preserved, abundant and diverse above the unexposed section, from -6.61 to 66.5 m, although preservation is poor above 59 m, coincident with the occurrence of greensand beds. The Waipawan/Mangaorapan boundary is identified at -3.99 m based on the lowest occurrence (LO) of *Morozovella crater*. The base of the Heretaungan stage is identified by the LO of the marker benthic species *Elphidium hampdenense* at 27.51 m, and the species is present up to 58.55 m. Two species of the genus *Morozovella*, *M. crater* and *M. lensiformis*, are present in all samples from -3.99 to 57.9 m and the genus is only absent in the uppermost Heretaungan sample (58.55 m). The primary datum for the Porangan Stage, benthic species *Elphidium saginatum*, is not identified in the section. The base of the Bortonian is identified by the primary datum, LO of *Globigerinatheka index*, directly above the unconformity at 59.71 m, and is supported by the LOs of *Bulimina bortonica* at 59.71 m and *Acarinina primitiva* at 63.05 m.

Planktic foraminiferal abundance is low in the early Waipawan (average 3%) but increases to >40% in the late Waipawan. Several pulses of high abundance, >70%, are seen in the early-middle Mangaorapan, whereas the late Mangaorapan has stable planktic abundance (Fig. 3). There is a general abundance drop in the Heretaungan, with the average value (38%) noticeably lower than in the Mangaorapan (65%).

5.1.3 Calcareous nannofossils

A summary of the detailed calcareous nannofossil biostratigraphy by Shepherd and Kulhanek (2016) is provided here. The presence of *Rhomboaster bramlettei* at -15.25 m places the base of the

section in Zone NP10, early Eocene (Fig. 3). The LO of *Sphenolithus radians* at -6.61 m is used as a secondary marker for the base of NP11 (Backman, 1986) rather than the index species *Tribrachiatus contortus*, which is absent. The LO of *Tribrachiatus orthostylus*, an event within the upper part of NP10 (Pälike et al., 2010), co-occurs with the LO of *S. radians*, suggesting the upper part of NP10 is within the non-exposed interval from -13.2 to -6.6 m. The LO of *Discoaster lodoensis* at -2.87 m, earliest Mangaorapan, marks the base of NP12. It is possible that *D. lodoensis* has a delayed LO at mid-Waipara, given that in the nearby Mead Stream section the LO of *D. lodoensis* occurs ~36 m below the LO of *Morozovella crater* and at mid-Waipara these two bioevents occur within ~1 m (Supp. Information Fig. 2). The HO of *T. orthostylus*, marker for the base of NP13, is observed at 11.13 m and lower Chron C22r (mid-Mangaorapan). The absence of *Discoaster sublodoensis*, marker for the base of NP14, means the NP13/NP14 boundary cannot be identified. However, the base of NP14 is known to occur in lower Chron C22n (Hollis et al., 2019), which is well-defined at mid-Waipara. From this we infer that the NP13/14 boundary lies in the late Mangaorapan, between ~20.7 and 27 m. Some or all of Zone NP15 (i.e., late Heretaungan–latest Porangan) is inferred to be missing because the markers for the base of NP15 and base of Subzone NP15b (LOs of *Nannotetrina fulgens* and *Chiasmolithus gigas*, respectively) are not observed. The base of NP16 is difficult to identify as both the primary and secondary markers, *Blackites gladius* and *Nannotetrina alata/fulgens*, are not observed. However, *Reticulofenestra umbilicus* (>14µm) and *Reticulofenestra reticulata* both have LOs in Zone NP16 (Pälike et al., 2010) and at mid-Waipara they co-occur at 62.26 m, early Bortonian. This suggests the lower part of Zone NP16 is missing, given that *R. reticulata* evolved at least several hundred thousand years after *R. umbilicus* (Gradstein et al., 2012; Agnini et al., 2014). Nannofossil and foraminiferal biostratigraphy agree that the unconformity at ~59 m encompasses the latest Heretaungan–earliest Bortonian (Fig. 3).

Nannofossil preservation is linked to carbonate content in this section. A positive correlation is observed between carbonate content and the visual observation of preservation (VOP), as well as the relative abundance of *Zygrhablithus bijugatus*, a species sensitive to dissolution (Jiang and Wise, 2009; Fig. 4). Poorly preserved assemblages occur in the Waipawan (NP10) and upper Heretaungan

(NP14) parts of the section where CaCO_3 is <10% and generally <15%, respectively. The best-preserved assemblages are in the Mangaorapan, from the base of Zone NP12 to NP13–lower NP14, where CaCO_3 is >15%. An increase in taxon richness and diversity is seen from the base of NP12, consistent with the increase in preservation. Overall, the covariance between preservation and diversity indices suggests preservation is an important factor influencing diversity in this section (Shepherd, 2017).

5.1.4 Dinoflagellate cysts

Dinocyst assemblages are generally abundant and well preserved. Integration of index taxa (Wilson, 1988; Morgans et al., 2004) with magnetostratigraphy and calcareous microfossil biostratigraphy allows the age control of key species to be improved (Fig. 3). In the Waipawan, the LOs of several zonal taxa are recorded: *Samlandia delicata* (NZE2a, -15.25 m) and *Impagidinium cassiculum* (NZE2b, -13.20 m) occur in nannofossil Zone NP10, whereas the LO of *Dracodinium waipawaense* (NZE3) is in Zone NP11 (-6.61 m). The range of *Wilsonidium ornatum* (NZE4) is restricted to the Mangaorapan (Zone NP12 to NP13; -2.87–17.83 m). The LOs of key taxa *Charlesdowniea coleothrypta* (19.98 m) and *Charlesdowniea edwardsii* (22.14 m) occur in the late Mangaorapan. The HO of *C. coleothrypta* (26.75 m) is in upper Chron C22n, close to the Mangaorapan/Heretaungan boundary, and the HO of *C. edwardsii* is early Heretaungan (32.40 m). The onset of common–frequent *Membranophoridium perforatum*, a regional bioevent (Wilson, 1984, 1988), occurs in the Heretaungan close to the Chron C21r/C21n boundary.

Additional taxa offer potential to further refine the early–middle Eocene zonation. The LO of *Impagidinium crassimuratum* and HO of *Manumiella rotunda* occur in Zone NP10 (early Waipawan). The LOs of *Membranophoridium perforatum*, *Schematophora obscura* and the genus *Homotryblum* are in Zone NP11 (late Waipawan). The LO of *Danea crassimuratum* is in Zone NP12 (early Mangaorapan). The LO of *Achilleodinium biformoides*, *Deflandrea antarctica* and *Impagidinium parvireticulum* are in Chron C22n (late Mangaorapan). The HO of the *Apectodinium* genus is close to the Chron C22r/C22n boundary, late Mangaorapan. Fewer bioevents are seen in the Heretaungan.

Endemic Antarctic Community taxa (Bijl et al., 2011), *Alterbidinium assymmetricum* and *Spinidinium macmurdoense*, have LOs in lower Chron C21r, correlated with Zone NP14.

5.1.5 Spores and pollen

Spore and pollen abundance ranges from 22–43% of the total palynomorph assemblage. Three zones (Raine, 1984; Morgans et al., 2004) are identified: PM3b, MH1 and MH2 (Fig. 3). The lower part of the section (-16.15 m to -13.2 m) is correlated with the earliest Eocene PM3b Zone, based on thermophilic taxa *Cupanieidites orthoteichus* and *Spinizonocolpites prominatus*, and rare *Myricipites harrisii* (Raine et al., 2009; Handley et al., 2011). The base of Zone MH1, defined by a noticeable increase in *M. harrisii* abundance, occurs between -13.2 m and -6.61 m (late Waipawan). *M. harrisii* is common–abundant from this level to the late Heretaungan (57.93 m) and this interval is correlated with Zone MH1. The tropical-subtropical spore *Crassoretitritetes vanraadshooveni* (*Lygodium*) has a HO in the late Mangaorapan. The overlying Bortonian interval is correlated with Zone MH2 based on the presence of *Nothofagidites flemingii*.

5.2 Carbonate content, and carbon and oxygen isotopes

Carbonate (CaCO_3) content is relatively low in the mid-Waipara section, never >30% (Fig. 5a). It is <15% in the earliest Eocene (early Waipawan) and most of the middle Eocene (Heretaungan–early Bortonian). The highest CaCO_3 values, albeit variable, are in the late Waipawan and Mangaorapan (early Eocene), also where well-preserved and abundant calcareous microfossil assemblages are recovered. The primary source for CaCO_3 in this section is assumed to be calcareous nannofossils. Variation in the relative abundance of planktic foraminifera suggests that the secondary source may vary from calcareous benthic foraminifera in the early Waipawan and Heretaungan–Bortonian, to planktics in the Mangaorapan. CaCO_3 content has a weak negative correlation with bulk carbonate $\delta^{13}\text{C}$ ($r = -0.25$, $n = 68$, $p < 0.05$), is not correlated with $\delta^{18}\text{O}$, and has a strong positive correlation with TEX_{86} ($r = 0.60$, $n = 68$, $p < 0.001$). Under typical ocean conditions, benthic

foraminifera will have lower $\delta^{13}\text{C}$ values than planktic foraminifera because the biological carbon pump delivers ^{12}C -enriched organic matter to the sea floor.

Bulk carbonate $\delta^{13}\text{C}$ values range from -0.8‰ to 1.6‰, with a general trend towards higher values from early to middle Eocene (Fig. 5b). A positive excursion, of ~1‰, occurs in the earliest Eocene (early Waipawan). The most negative $\delta^{13}\text{C}$ value in the section, -0.8‰, is recorded at -6.61 m in the late Waipawan, Zone NP11, and marks the first of a series of six (#1–6) negative carbon isotope excursions (CIEs) in the Waipawan–Mangaorapan (early Eocene), which are superimposed on a positive $\delta^{13}\text{C}$ trend. The $\delta^{13}\text{C}$ minimum within each CIE also increases over time, from -0.7‰ at -2.12 m to 0.7‰ at 26.75 m. A baseline positive shift (0.7–1.5‰) is recorded across the Mangaorapan/Heretaungan boundary. Through most of the Heretaungan $\delta^{13}\text{C}$ values remain stable, although a shift to lower values occurs in the late Heretaungan between ~50 and 59 m. The Bortonian section is marked by variable $\delta^{13}\text{C}$ values, from -0.2‰ to 1.4‰, with a possible negative CIE at 62.26 m. The CIEs tend to be associated with lower CaCO_3 values but not in all cases (e.g., CIEs #3 and #5). Some of the negative shifts in $\delta^{13}\text{C}$ in the earliest Waipawan and Heretaungan may be partly due to the low abundance of planktic foraminifera, because benthic foraminiferal calcite is generally more enriched in ^{12}C . However, the lack of a consistent relationship between the CIEs in the late Waipawan and Mangaorapan and planktic abundance suggests that foraminiferal calcite is not the primary source of carbonate in this interval.

The bulk carbonate $\delta^{18}\text{O}$ record is not correlated with other geochemical proxies (Appendix, Supp. Information Fig. 3) and the general trend is inconsistent with other early Eocene $\delta^{18}\text{O}$ records (e.g., Westerhold et al., 2018; Barnett et al., 2019). Values in the range of -2.5 to -4‰ yield temperatures in the range of 22–30°C, which are consistent with SSTs reported in previous studies (Hollis et al., 2009, 2012). However, these values are interspersed with $\delta^{18}\text{O}$ values that range from -4 to -6.4‰ and yield unrealistically hot temperatures (up to 42°C). These values are likely to result from post-depositional interactions with ^{18}O -depleted meteoric water (Hollis et al., 2012). Because we have no way of discriminating between reliable and unreliable values, the bulk oxygen $\delta^{18}\text{O}$ record is

not discussed further in this article. The bulk carbonate $\delta^{13}\text{C}$ record is not affected by meteoric water interactions.

5.3 GDGT distributions

Both isoprenoidal and branched GDGTs are present in all samples, and the TEX_{86} and BIT records are broadly consistent with previously reported Eocene records from this section (Hollis et al., 2009, 2012). The most notable change in the TEX_{86} record is in the basal part of the section, where values increase from 0.65–0.7 in the early Waipawan to >0.8 in the late Waipawan (Fig. 5c). These high TEX_{86} values continue up to 5.23 m in the early Mangaorapan (Chron C23n.2n). The overlying TEX_{86} record is characterized by a gradual decline into the middle Eocene, with a sharp decrease at the Mangaorapan/Heretaungan boundary. Average TEX_{86} values in the Heretaungan are lower (0.7) than in the Mangaorapan (0.8). TEX_{86} values in the early Bartonian, Zone NP 16, are variable and range between 0.55 and 0.7. There is a strong negative correlation ($r = -0.54$, $n = 68$, $p < 0.001$) between TEX_{86} and bulk carbonate $\delta^{13}\text{C}$. Most early Eocene CIEs appear to be associated with higher TEX_{86} , implying that these CIEs represent hyperthermals.

The methane index (MI) is ≤ 0.30 in all samples, indicating that TEX_{86} values are not biased by a large contribution of methanogens to the GDGT pool. Low BIT indices (<0.25) throughout the section indicate that TEX_{86} values are likely not significantly biased by terrestrial input. BIT values are lowest (<0.1) in the Waipawan and increase progressively through the overlying Mangaorapan and Heretaungan Stages (Fig. 5d). The BIT index is highly variable in the early–middle Mangaorapan (Zone NP12), with lower values associated with the hyperthermals (high TEX_{86}) and higher values associated with positive excursions in bulk carbonate $\delta^{13}\text{C}$. Overall, the BIT index exhibits a weak negative correlation with TEX_{86} and a strong positive correlation with $\delta^{13}\text{C}$ ($r = -0.24$, $p < 0.05$ and 0.65 , $p < 0.001$, respectively, $n = 68$). The anticorrelation between the BIT index and $\delta^{13}\text{C}$ is difficult to interpret, if we assume the BIT index purely reflects changes in terrestrial input, particularly the decrease in BIT and, hence, terrigenous supply during the negative CIEs. Previous studies in Eocene sections to the north (Marlborough, Fig. 1) have shown that hyperthermals are associated with

increased terrigenous input in bathyal settings (Hollis et al., 2005a; Nicolo et al., 2007; Slotnick et al., 2012, 2015), and this would be expected to be associated with an increase in BIT values. At mid-Waipara, however, we observe a decrease in BIT values during negative CIEs, which implies reduced terrigenous input and may be a localised response to transient climate events, such as current winnowing of finer sediments. However, the BIT index can be influenced by other factors and does not always purely represent a simple two end-member model between pure marine and terrestrial input. For example, the reduced BIT could reflect a relative increase in crenarchaeol over brGDGT input during the hyperthermals, or the BIT may respond to changes in the contribution of *in situ* produced brGDGTs to the sedimentary GDGT pool. Either way, the low BIT values indicate that a relatively low amount of the GDGT pool is derived from soils.

The brGDGTs found in these marine samples (Appendix) could also contain brGDGTs generated in the water column or marine sediments, rather than from land-based soils, which complicates the use of brGDGTs in these sediments to quantify terrestrial temperature (De Jonge et al., 2014b; Sinninghe Damsté, 2016). A non-soil source of brGDGTs to the sediments at mid-Waipara is further supported by the observation that the relative abundance (%) of penta- or hexamethylated versus tetramethylated brGDGTs is higher than that seen in any modern mineral soil or peat (Supp. Information Fig. 4). The number of rings of pentamethylated brGDGTs versus the number of rings of hexamethylated brGDGTs is also significantly higher than that seen in any modern mineral soil or peat. We therefore do not discuss brGDGT-based terrestrial temperatures at mid-Waipara River.

5.4 The Early Eocene Climatic Optimum in the mid-Waipara River section

A combination of biostratigraphy, magnetostratigraphy, bulk carbonate $\delta^{13}\text{C}$ values and TEX_{86} is used to determine the position of the EECO in the mid-Waipara section. As discussed earlier, the EECO is inferred to extend from 53.26–49.14 Ma, Chron C24n.2r (J event, mid-NP11) to uppermost Chron C22n (C22nH5 event, lower NP14) (Westerhold et al., 2018). The lowest chron identified in mid-Waipara is C23.2n, which lies in Zone NP12 (Fig. 5). The interval directly overlying the unexposed interval in the lower part of the section (Waipawan, -6.61 m) is correlated with NP11,

has the highest TEX_{86} values in the section, and also has what we infer to be the first of six CIEs in the section. For these reasons, we place the base of the EECO at this level (Fig. 6). There are uncertainties, however, constraining the age of the lower part of the section (Supp. Information Fig. 2), and we infer the CIE at this level (#1) to correspond with either the J event (C24n.2rH1) or the K event (C24n.1nH1). The upper limit of the EECO in this section is well recorded. We place it at the uppermost CIE (#6), which lies within upper Chron C22n and coincides with the onset of a cooling trend in the TEX_{86} record (Fig. 5). Given the age of the Mangaorapan/Heretaungan boundary, at 49.27 Ma (C22n(0.6)) and magnetostratigraphy in this part of the section, we infer CIE #6 to correspond with the C22nH4 event (49.25 Ma). This suggests that cooling at mid-Waipara began slightly earlier than the top EECO as recognised by Westerhold et al. (2018) at 49.14 Ma (C22nH5).

Combining these two datums with the integrated magnetobiochronology for the section (Appendix, Supp. Information), calibrated to the timescale of Westerhold et al. (2017), allows us to provisionally correlate the other CIEs in the section as follows: #2 = C23rH2 or M event; #3 = C23n.2nH2 or O event; #4 = C22rH1 or Q event; #5 = C22rH4 or T event (Fig. 6). The major positive shift in $\delta^{13}\text{C}$ during C23n (51.2–51 Ma; Westerhold et al., 2018) is not clearly observed at mid-Waipara, perhaps due to the presence of cryptic unconformities in this part of the section.

5.5 Paleoenvironmental changes

5.5.1 Foraminiferal assemblage

Benthic foraminiferal paleodepth indicators (e.g. *Pleurostomella*, *Stilostomella* and *Bathysiphon* spp.) suggest that the entire section was deposited in a middle bathyal setting (Appendix, Supp. Information). The incoming of *Nuttallides carinotrumpyi* and the genera *Karreriella* and *Vulvulina* in the early EECO (late Waipawan and early Mangaorapan) indicate a deeper bathyal setting. The presence of *Tritaxilina zealandica*, from mid EECO to earliest post-EECO (middle Mangaorapan–early Heretaungan), suggests that this is the deepest interval in the section, probably lower bathyal (Hayward, 1986; Hayward et al., 2010). Foraminiferal assemblages higher in the post-

EECO Heretaungan indicate shallowing with the disappearance of *Karreriella* and *T. zealandica*, although middle bathyal indicators persist into the Bortonian.

Foraminiferal assemblages are affected by preservation. The best-preserved assemblages are in the late Waipawan–Mangaorapan (EECO) where CaCO_3 content is highest. Planktic abundance (Fig. 3) is also correlated with carbonate content (CaCO_3 , $r = 0.76$, $n = 26$, $p < 0.001$) although this may be due to a combination of factors, such as improved preservation and warmer conditions. Peaks in planktic abundance align with three of the negative CIEs (#1, 2, 5) and may be directly related to warmer SST or indirectly linked to warming by increased clay content, which can enhance preservation (Hollis et al., 2019). However, we have not confirmed that CIEs in this section are accompanied by an increase in clay. A strong correlation with TEX_{86} ($r = 0.84$, $n = 26$, $p < 0.001$) provides further evidence that planktic abundance is linked to temperature. In the early Waipawan (below the EECO), a combination of cooler SST (Fig. 5c) and poor preservation perhaps led to low planktic abundance, despite the middle bathyal depositional setting. A similar trend is evident in the late Heretaungan.

5.5.2 *Dinocyst assemblage*

Gonyaulacoid dinocysts, representative of autotrophic dinoflagellates (Dale, 1996), dominate the Eocene assemblages and include the genera *Spiniferites*, *Operculodinium*, *Cerebrocysta* and *Impagidinium* (Fig. 7). Peridinioids (e.g., *Spinidinium* spp.), predominantly heterotrophic dinoflagellates, comprise <30% of the assemblage, apart from an interval in the late EECO (late Mangaorapan) where they become super-abundant. Assemblages below the EECO, early Waipawan, are dominated by cosmopolitan taxa, such as *Elytrocysta* spp., *Operculodinium* spp. and *Spiniferites* spp., and peridinioids are frequent. Compared with the early Waipawan, assemblages in the EECO (late Waipawan–Mangaorapan) are more diverse, with new taxa (e.g., *Batiacasphaera* spp., *Membranophoridium perforatum*, *Schematophora obscura*) becoming common, some cosmopolitan taxa (e.g., *Elytrocysta* spp., *Operculodinium* spp.) declining in abundance, and taxa such as *Diphyes* spp., *Hystriocholpoma* spp. and *Impagidinium cassiculum* increasing in abundance. The tropical–

warm temperate genus *Homotryblium* is frequent–abundant in the early and middle EECO, with three main abundance peaks ranging from 19–30%. In the late EECO, there is a significant increase (up to 40%) in peridinioid abundance, and they continue to be frequent–abundant in the overlying post-EECO Heretaungan. Early Bortonian samples are a mix of cosmopolitan and more endemic (e.g., *Enneadocysta*) taxa.

5.5.3 Spore and pollen assemblage

Spores and pollen average 37% of palynomorph assemblages below the EECO (Fig. 8). This abundance declines in the early–middle EECO, with a minimum value of 22% in Chron C22r, begins to increase in the late EECO, and increases slightly in the post-EECO Heretaungan. Spore and pollen abundance has a strong negative correlation ($r = -0.61$, $n = 35$, $p < 0.001$) with TEX_{86} and a moderate positive correlation ($r = 0.33$, $n = 35$, $p < 0.05$) with BIT index. The parallel trend of increasing terrestrial palynomorphs and BIT index in the late EECO and post-EECO Heretaungan suggests an increasing contribution of terrestrial material in the sedimentary record as temperatures cooled following the peak-EECO warmth.

Pre-EECO assemblages are dominated by gymnosperm pollen (up to 71%), particularly *Podocarpidites* and the Araucarian taxon *Dilwynites granulatus*, and *Cyathidites* fern spores (Fig. 8). In contrast, the early EECO shows a marked increase in angiosperm pollen, from <15% in the early Waipawan up to 44% in the early Mangaorapan, and a concomitant decline in gymnosperm abundance, most notably *Podocarpidites*. This angiosperm increase is mainly driven by a rise in Casuarinaceae (*Myricipites harrisii*), although other angiosperms become more common, including *Malvacipollis subtilis*, *Proteacidites* and *Tricolporopollenites latizonatus*. Vegetation remains relatively stable in the EECO, with only a minor increase in *D. granulatus* and *Podocarpidites* gymnosperms in the late EECO. The abundance of *M. harrisii*, and total angiosperms, decline slightly in the Heretaungan and continue to decline in the early Bortonian, along with the incoming of the cooler southern beech family Nothofagaceae genus *Nothofagus* (*Nothofagidites flemingii*).

5.6 Microfossil paleotemperature indicators

The relationship between microfossil assemblages and latitudinally constrained environmental parameters, such as temperature and salinity, has been widely used to define biogeographic zones, both in the modern ocean (e.g., McIntyre and Bé, 1967; Okada and Honjo, 1973; Prebble et al., 2013; Zonneveld et al., 2013) and in the geological record (e.g. Haq, 1981; Hennissen et al., 2017). Whilst many environmental parameters have the potential to influence microfossil distribution, SST has been shown to be the most important variable for calcareous nannofossil (e.g., Haq et al., 1977; Haq, 1981; Wei and Wise, 1990) and dinocyst assemblages (e.g., De Vernal et al., 2005; Sluijs et al., 2005; Prebble et al., 2016; Frieling and Sluijs, 2018).

Warm-water indicators in the calcareous nannofossil assemblage, namely *Discoaster* spp., *Sphenolithus* spp. and *Coccolithus formosus*, are most abundant in the early and middle EECO, with a combined abundance up to 19% (Fig. 4). The combined abundance of this warm-water group is also high in the early Waipawan, below the EECO, and in the latest Heretaungan, post-EECO. This, however, is due to the high preservation potential of *Discoaster* spp., which dominates the warm-water assemblage in these intervals. In the EECO, cool-water indicators comprise <8% of the assemblage, and they become more abundant (up to 17%) in the post-EECO Heretaungan. Initially, the increase in cool-water taxa is related to an increase in *Reticulofenestra daviesii*, which is followed by an increase in *Chiasmolithus* spp. in the late Heretaungan. The cool-water group has a moderate negative correlation ($r = -0.43$, $n = 30$, $p < 0.02$) with TEX_{86} , whereas the warm-water group has a weak positive correlation ($r = 0.30$, $n = 30$, $p < 0.1$); the weaker correlation is likely due to the preservational effects noted above.

The abundance and diversity of the warm-water Wetzelielloideae dinocyst group is highest in the EECO, comprising up to 7% of the assemblage and 7 taxa, and the group disappears entirely in the post-EECO (Fig. 7). The warm temperate–tropical genus *Homotryblum* is first seen in the earliest EECO and is abundant (up to 30%) in the early and middle EECO, and generally lower in the post-EECO. The warm-water Wetzelielloideae group has a strong positive correlation ($r = 0.59$, $n = 41$, p

<0.001) with TEX₈₆, and there is a weak positive correlation ($r = 0.29$, $n = 41$, $p < 0.1$) between *Homotryblum* and TEX₈₆. Taxa of the Endemic Antarctic Community (EAC) group are first noted in the late EECO, with abundance progressively increasing (up to 17%) in the post-EECO. The EAC group has a strong negative correlation ($r = -0.56$, $n = 41$, $p < 0.001$) with TEX₈₆. These correlations between calcareous nannoplankton and dinocyst fossil assemblage-based proxies for temperature and the independent SST proxy, TEX₈₆, provide convincing evidence that both approaches are reliable guides to past water temperature.

The main vegetation change is an increase in angiosperm pollen, driven by a rise in Casuarinaceae (*Myricipites harrisii*) in the early EECO (Fig. 8). *M. harrisii* abundance has a strong positive correlation with TEX₈₆ ($r = 0.76$, $n = 33$, $p < 0.001$). Angiosperms with affinities to mesothermal–megathermal climates, such as *Anacolosidites*, *Bluffopollis scabratus*, *Intratropipollenites notabilis* and *Margocolporites cribellatus*, are rare but occur below, in, and above the EECO (Appendix, Supp. Information). Most of these taxa do not occur in the cooler early Bortonian, but the thermophilic *Spinizonocolpites prominatus* (*Nypa* mangrove) and *Malvacipollis subtilis* taxa continue to be present.

5.7 Sea-surface temperature

While the evidence above, as well as numerous other multiproxy studies, show that TEX₈₆ is a robust guide to relative changes in SST (e.g., Zachos et al., 2005; Pearson et al. 2007), there is ongoing debate about how the proxy relates to absolute temperature in the Paleogene, and especially to mean annual SST in middle–high latitudes (Hollis et al., 2012). Here we use the two most widely used calibrations, TEX₈₆^H (Kim et al., 2010) and BAYSPAR_{SST} (Tierney and Tingley, 2015), which yield similar absolute values in this record (Fig. 9a). TEX₈₆^H is based on an exponential relationship with SST whereas BAYSPAR assumes a linear relationship, which results in higher values at the upper end of the calibration (i.e. where TEX₈₆ > 0.7) and especially beyond the range of the modern calibration dataset. In our record, the amplitude of SST change is larger in BAYSPAR_{SST} than in TEX₈₆^H (Fig. 9b).

The most marked shift in SST is in the Waipawan, from pre-EECO to early EECO, with an increase of between ~7 and 12°C (Fig. 9b). BAYSPAR SST increases from ~22.5 to 35.5°C, whereas TEX₈₆^H SST increases from ~26 to 33.5°C. SST is highest in the early EECO and declines slightly through the middle and late EECO. The baseline shift to a lower SST in Chron C23n.2n (~5.2 m), corresponding with the C23n.2nH2 or O Event (Fig. 6), matches North Pacific records that indicate the end of the warmest interval in the EECO occurs in uppermost Chron C23n.2n at 51.23 Ma (Westerhold et al., 2018). A decrease in TEX₈₆-derived SST occurs across the Mangaorapan/Heretaungan boundary, and SST continues to decline in the post-EECO Heretaungan. Lower SST is present in the early Bartonian (middle Eocene, Zone NP16), although a transient peak, up to 25.2°C (BAYSPAR_{SST}) and 27.9°C (TEX₈₆^H), is recorded and may represent the Middle Eocene Climatic Optimum (MECO) at ~40 Ma.

5.8 Red Sea-type GDGT distributions

The %GDGT_{RS} distribution is used to identify sediments with unusually low amounts of GDGT-0 relative to crenarchaeol regioisomer, which is characteristic for the GDGT distribution found in modern sediments from the Red Sea (Trommer et al., 2009). Where %GDGT_{RS} >30 it is inferred that the distribution is similar to that found in the Red Sea and may have added a warm bias to SST estimates (Inglis et al., 2015). %GDGT_{RS} values >30 are common during times of elevated warmth but may be a response to factors other than temperature given the distinct Red Sea archaeal assemblages (Trommer et al., 2009). Crucially, the modern Red Sea data exert a particularly strong influence on the high temperature end of all TEX₈₆-SST calibrations, depending on how they are included (Inglis et al., 2015). At mid-Waipara River, %GDGT_{RS} values >30 are consistently observed in the EECO, with the highest values in the early and middle EECO (Fig. 9c). %GDGT_{RS} values drop to <30 across the Mangaorapan/Heretaungan boundary. %GDGT_{RS} values are <30 in the early Waipawan (pre-EECO), Heretaungan (post-EECO) and early Bartonian.

6. Discussion

6.1 Comparison of proxy-based SST and microfossil records in the early and middle Eocene

Many early Paleogene studies have attempted to integrate climate proxy data with climate model simulations to understand global climate and carbon cycle response to elevated temperatures and greenhouse gases. While progress has been made in reconciling proxy temperature reconstructions with climate model simulations (Carlson and Caballero, 2017; Naafs et al., 2018), there remain known problems and inconsistencies with geochemical-based temperature proxies (Hollis et al., 2012, 2019). Multiproxy SST reconstructions (Mg/Ca ratios and $\delta^{18}\text{O}$ values of foraminiferal tests and GDGT-based TEX₈₆ values) have been completed for the early–middle Eocene at mid-Waipara (Hollis et al., 2009, 2012; Inglis et al., 2015). The new TEX₈₆-based SST record presented here validates and complements these previous reconstructions (Fig. 10). The absolute SST values, however, remain debatable because they imply a reduced latitudinal temperature gradient between middle and low latitudes in the EECO and into the post-EECO, compared to the present (Cramwinckel et al., 2018; Naafs et al., 2018). In this context, the particularly warm temperatures (>30°C) in the Southwest Pacific warrant further investigation. Microfossil assemblages offer a means to explore these geochemical-based SST proxies and assess the faunal/floral evidence for tropical SSTs during the EECO in mid-latitudes (paleolatitude ~46°S) of the Southwest Pacific. We have found a good correlation between the trends in the TEX₈₆ SST proxy and water temperature indicators within calcareous nannofossil and dinocyst assemblages.

Comparison of early–middle Eocene nannofossil assemblages from mid-Waipara with coeval records from subtropical (Shatsky Rise), temperate (Exmouth Plateau and Campbell Plateau) and subpolar (Kerguelen Plateau) provinces indicate that mid-Waipara assemblages are most similar to the other temperate sites, rather than assemblages at the subtropical setting (Fig. 11). Warm-water taxa (*Coccolithus formosus*, *Discoaster* spp., *Sphenolithus* spp.) are most abundant in the EECO at mid-Waipara, reaching up to 19% of the total assemblage. This is comparable with Site 762 (paleolatitude ~38°S), Exmouth Plateau, where warm-water taxa comprise up to 24% in the EECO (Schneider et al., 2011), and Site 277 (paleolatitude ~54°S), Campbell Plateau (Shepherd, 2017). Warm-water taxa at

the subtropical Site 1210 (paleolatitude $\sim 28^{\circ}\text{N}$), Shatsky Rise, comprise up to 49% in the EECO (Schneider et al., 2011). Indeed, there is a three-fold increase in the abundance of warm-water taxa in the EECO between mid-Waipara (average 11%) and Site 1210 (average 35%). Conversely, cool-water taxa (*Chiasmolithus* and *Reticulofenestra* spp.) are notably more abundant in the EECO, up to 18%, at the polar Site 1135 (paleolatitude $\sim 59^{\circ}\text{S}$), Kerguelen Plateau (Schneider et al., 2011), compared to $<10\%$ at mid-Waipara, Campbell Plateau and Exmouth Plateau temperate sites. Cool-water taxa do not significantly increase in abundance at mid-Waipara and Site 277 until after the EECO (Fig. 11).

Dinocyst assemblages at mid-Waipara exhibit a trend that is comparable to nannofossil observations. The abundance and diversity of the warm-water Wetzelielloideae group is highest in the EECO but the group comprises only a minor component ($<10\%$) of the total assemblage (Fig. 12e). It is estimated the lower SST tolerance of Wetzelielloideae was $20 \pm 2.5^{\circ}\text{C}$ (Frieling et al., 2014, Frieling and Sluijs, 2018). Representatives of the Wetzelielloideae group are present below the EECO and the group disappears above the EECO; however, TEX_{86} -based SST is well above 20°C in this Waipawan–Heretaungan interval (Fig. 12b). This suggests that the disappearance of the group may be linked to other factors in addition to cooling, such as changes in nutrients or fresh-water input. The warm temperate–tropical genus *Homotryblum* peaks in abundance, up to 30%, in the lower–middle EECO. The continued presence of *Homotryblum* above the EECO and in the early Bartonian indicates a tolerance to a broader SST range than the Wetzelielloideae group, in contrast to suggestions it preferred SSTs $>25^{\circ}\text{C}$ (Frieling and Sluijs, 2018), or perhaps an evolutionary adaptation to post-EECO cooling (e.g., Dybkjær, 2004). The high *Homotryblum* abundance in the EECO may be due to a combination of high SST and specific surface-water conditions (see section 6.3). The cooler-water EAC group first appear at mid-Waipara in the late EECO and, as with nannofossils, become more common in the post-EECO (Fig. 12d, e). The increase in these cooler-water groups suggests that the temperature gradient between the middle and low latitudes was increasing in the post-EECO middle Eocene, perhaps related to tectonic processes such as the deepening of the Tasmanian Gateway (Bijl et al., 2013b; Sijp et al., 2016).

Calcareous and organic marine microfossils from mid-Waipara show that elements of low-latitude provinces existed in the early Eocene in the New Zealand region and became more diverse and abundant in the EECO, but that marine assemblages characteristic of low-latitude Eocene oceans were by no means dominant in the extended period of early Eocene warmth. In fact, nannofossil assemblages indicate that temperature gradients between mid- and low-latitudes in the EECO were greater than indicated by geochemical SST proxies. In the EECO, there are three times as many warm-water indicators in the nannofossil assemblage at the low-latitude Shatsky Rise site (average 35%) as there are at the mid-latitude mid-Waipara section (average 11%). This is in contrast with geochemical-based SST proxies, where average SSTs in the EECO only differ by 5°C across the same latitudinal range and climate zones.

Despite these apparent discrepancies between absolute temperature inferred from geochemical proxies and fossil biogeography, microfossil assemblages and SST proxies are in good agreement in the trend of relative temperature change in the early–middle Eocene. TEX₈₆-based records indicate pronounced warming of between ~7 and 12°C (Fig. 9) from pre-EECO to early EECO. This is also associated with the most notable biotic change in the section, including the highest abundance of warm-water taxa and % planktic foraminifera (Fig. 12 d, e), increasing nannofossil and dinocyst diversity, and a long-term shift to more abundant and diverse angiosperm vegetation (Fig. 7). Declining SST from late EECO to post-EECO is mirrored with an increasing abundance of cool-water nannofossil and dinocyst taxa, although terrestrial vegetation shows little change in the post-EECO Heretaungan. It is not until the Bortonian that cooler temperatures are indicated by the rise in abundance of the Nothofagaceae, southern beech, family.

6.2 Early and middle Eocene sedimentation changes

Early Eocene extreme warming events are commonly linked with increased accumulation of terrigenous material on continental margins, including New Zealand, due to an enhanced hydrological cycle that promoted both chemical and physical weathering processes and transport of terrigenous sediment into adjacent basins (Dickens et al., 1997; Schmitz and Pujalte, 2007; Carmichael et al.,

2017). This is well-documented for the short-lived PETM, which is also associated with notable changes in sedimentation patterns and marine primary productivity (Crouch et al., 2003; Nicolo et al., 2007; Giusberti et al., 2016). Equivalent EECO records are sparse, making it difficult to compare the climatic impacts on sedimentation between transient and long-term warming events. In New Zealand, the Mead and Branch Stream (Fig. 1) records suggests similar changes in terrigenous delivery and sedimentation occurred in the EECO to that documented for the PETM, with an increased component of terrigenous-sourced clay during early Eocene CIEs, as well as in the EECO, and highest sediment accumulation rates (SARs) during the EECO (Slotnick et al., 2012, 2015; Dallanave et al., 2014).

At mid-Waipara, SARs also appear to have increased at the base of the EECO (from ~4 to 10 m/Myr), peaked in the latest EECO (14 m/Myr), and then stabilised through the overlying post-EECO Heretaungan (~10 m/Myr; Dallanave et al., 2016). However, SAR estimates are uncertain for the base of the section due to limited exposure, and in the late Heretaungan due to likely erosion at the overlying unconformity (~59 m). The SAR is generally much higher at Mead Stream (Dallanave et al., 2014), despite the sediments being primarily pelagic carbonate and hemipelagic clays; background SAR is 20 m/Myr and peak SAR in the EECO is 40–100 m/Myr at Mead Stream. This indicates that the Eocene section at mid-Waipara is relatively condensed and that cryptic unconformities may be present, which would distort the estimates of SAR.

Two other commonly used proxies for terrigenous input in marine sediments, the BIT index and terrestrial palynomorph abundance (Fig. 12f), exhibit opposing trends in the lower part of the early Eocene. This may be related to other factors influencing the BIT index, as discussed above (section 5.3). However, the convergence of trends in the mid–late EECO and post-EECO Heretaungan suggests that cooling is linked to increased terrigenous input in this section.

In this respect, the mid-Waipara record differs from Mead Stream, where a notable increase in accumulation of terrigenous material is associated with the long-term EECO. This is further emphasised by differences in thickness of the EECO at the two sections: 34 m at mid-Waipara versus >100 m at Mead Stream (Supp. Information Fig. 2). Benthic foraminiferal assemblages indicate both sections were deposited at bathyal depths in the early Eocene. Studies of the eastern Marlborough

pelagic succession (Reay, 1993; Hollis et al., 2005b) show that Mead Stream is the thickest, and most distal, Paleocene–Eocene section of an oceanic carbonate ramp succession. Sections closer to the paleo-shoreline are thinner, with major unconformities truncating the succession in this proximal area. A similar relation may apply to Mead and mid-Waipara sections, with Mead being in a distal depocenter for terrigenous weathering products in the EECO, whereas mid-Waipara represents a more dynamic coastal setting, where climatic changes cause changes in sediment delivery pathways and result in a more complex relationship between SAR and other indicators of terrigenous supply, sea level change and climate.

6.3 Early and middle Eocene changes in marine productivity and surface water conditions

Marine microfossils can provide insight into surface productivity and nutrient availability. Peridinioid dinocysts, predominantly heterotrophic dinoflagellates, make up <20% of the assemblage in the lower–mid EECO, and the abundance peak (40%) in the late EECO is coincident with an increase in the BIT index and terrestrial palynomorph abundance (Fig. 12f, g). Peridinioid abundance is <30% of the assemblage in the post-EECO. The lowest peridinioid abundance is associated with the negative CIEs and high SST (correlation $r = 0.39$, $p < 0.02$ and $r = -0.3$, $p < 0.01$, $n = 43$, with $\delta^{13}\text{C}$ and TEX_{86} , respectively).

Several short-lived abundance peaks, up to 30%, of the genus *Homotryblum* in the early and middle EECO (Fig. 12e) suggest the presence of seasonally elevated salinity levels and/or surface water stratification (Frieling and Sluijs, 2018). *Homotryblum* is morphologically like the extant euryhaline species *Polysphaeridium zoharyi*, which occurs in low–mid latitudes and is tolerant to extreme salinities and shallow water depths (Edwards and Anderle, 1992; Reichart et al., 2004). Most studies suggest *Homotryblum* has an affinity to hypersaline environments (Köthe, 1990; Pross and Schmiedl, 2002), although there is a possibility the genus favoured low-salinity conditions (Dybckjær, 2004). Whilst super-abundant *Homotryblum* is commonly linked with lagoonal/restricted inner marine settings (e.g., de Verteuil and Norris, 1996), benthic foraminiferal assemblages show the Ashley Mudstone was deposited at bathyal depths. The *Homotryblum* peaks do not correlate with

inner neritic dinocyst increases (e.g., *Cordosphaeridium*, *Glaphyrocysta*; Fig. 7), suggesting the surface water conditions that led to *Homotryblum* blooms were not restricted to a coastal setting but extended into the Canterbury Basin. The EECO *Homotryblum* peaks correspond with high SST and %GDGT_{RS} values >30 (Fig. 12 b, c), and partly correlate with CIEs (#3 and #4) and peaks in warm-water nannofossils (Figs. 12a, d). Elsewhere, high %GDGT_{RS} values (>30) are seen in times of elevated warmth (PETM and EECO) from the North Sea Basin, New Jersey margin and SW Pacific sites that have coeval high abundances of epicystal Goniodomidae dinocysts, such as *Eocladopyxis*, *Polysphaeridium* and *Homotryblum* (Sluijs and Brinkhuis, 2009; Inglis et al., 2015; Frieling and Sluijs, 2018). In New Zealand, abundant *Homotryblum* is also noted in the EECO at Mead Stream (Cooper, 2018) and Hampden Beach (Inglis et al., 2015).

While deciphering the influence of productivity on nannofossil assemblages is complicated by the interconnectivity between temperature and nutrient availability (Agnini et al., 2007; Schneider et al., 2011), some general observations indicate that surface productivity at mid-Waipara did not increase in the EECO. Rather, the EECO is characterised by the replacement of one mesotrophic genus, *Toweius*, with another, *Reticulofenestra*, which occurs in the late EECO and is coeval with the peridinioid abundance peak and increasing BIT values and terrestrial palynomorph abundance (Fig. 12f, g). The combined abundance of *Toweius* and *Reticulofenestra* is lower in the EECO (average 46%) than it is below or above the EECO (average 65% and 55%, respectively).

At the oceanic bathyal Mead Stream, there is evidence for increased terrigenous-sourced clay content and SARs in the EECO (Slotnick et al., 2012; Dallanave et al., 2015), but no clear signal of enhanced marine surface productivity. A marked decline in radiolarian abundance and diversity, and low diatom abundance, imply a decrease in biosiliceous productivity linked with the EECO (Hollis, 2006). Rather, assemblages characteristic of oligotrophic, possibly stratified, conditions prevailed. Open ocean gonyaulacoid taxa dominate dinocyst assemblages in the EECO, and super-abundant *Homotryblum* occurs in an interval corresponding with the J-event (EECO onset; Cooper, 2018).

6.4 Early Eocene vegetation change

In New Zealand, the most notable long-term vegetation shift in the early Eocene is the widespread abundance increase in Casuarinaceae pollen of *Myricipites harrisii* (Raine, 1984; Pocknall, 1990; Crouch and Brinkhuis, 2005). The precise timing is poorly constrained due to difficulties in accurately dating terrestrial sediments and correlation with well-calibrated marine sections (Morgans et al., 2004; Raine et al., 2009; Handley et al., 2011). The vegetation shift has been correlated with middle–late Waipawan, nannofossil Zone NP11 and dinocyst zone NZE3 (Crouch and Brinkhuis, 2005), but a direct link with Eocene climatic changes has not been made until this study.

Our results provide the clearest evidence to date that the Casuarinaceae increase is correlated with EECO warming. The increase in *M. harrisii* abundance is in the late Waipawan (Fig. 8), and corresponds with the warmest SST in the early EECO (Fig. 12b). Casuarinaceae remain frequent–abundant in the EECO, and whilst there is a gradual decline in abundance post-EECO, the duration of common–abundant *M. harrisii* continues at least 4–5 Myr above the EECO and into the middle Eocene Porangan Stage (Raine et al., 2009).

Pollen of *M. harrisii* is first seen in New Zealand and Australia in the early–middle Paleocene (Raine, 1984; Macphail et al., 1994; Contreras et al., 2014), but is relatively sparse until the early Eocene. Whilst *M. harrisii* is common or abundant in New Zealand in the early–middle Eocene, the southern Australia record is varied: high abundances occur in the Australo-Antarctic basins (e.g., Otway Basin) but not in Southeastern Australia (e.g., Gippsland Basin), where gymnosperm pollen remain abundant (Harris, 1965; Carpenter et al., 2012; Contreras et al., 2014; Holdgate et al., 2017). Casuarinaceae is a family characteristic of sclerophyllous, seasonally dry forests, but also includes the primitive genus *Gymnostoma*, a tropical–subtropical rainforest margin taxon adapted to low nutrient soils (Hill, 1994; Prider and Christophel, 2000; Steane et al., 2003). Fossil pollen of *Gymnostoma* and *Casuarina* are virtually indistinguishable, apart from the latter being generally larger (Kershaw, 1970). Whilst macrofossil evidence suggests *Gymnostoma* was common in the early Paleogene (Christophel, 1980; Hill, 1994; Greenwood and Christophel, 2005), the earliest macrofossil record of *Casuarina* is less clear, perhaps in the Eocene, but the oldest definitive macrofossils are Oligocene (Greenwood and Christophel, 2005; McGowran and Hill, 2015). The ecological interpretation of *M.*

harrisii is therefore complicated by the possibility that pollen was produced by *Gymnostoma* and *Casuarina* plants.

A combination of causes may have led to the long-term increase in Casuarinaceae vegetation linked with the EECO in New Zealand. Firstly, transient extreme warming at the PETM did not have a notable effect on Casuarinaceae (Crouch and Brinkhuis, 2005), but longer-term warming associated with the EECO may have allowed for vegetation change to occur and become established. At mid-Waipara, EECO mean annual temperature (MAT) estimates have been calculated from spore and pollen assemblages, which range from $17.1 \pm 6.8^{\circ}\text{C}$ (bioclimatic analysis) to $22.6 \pm 1.4^{\circ}\text{C}$ (co-existence approach) in the EECO (Pancost et al., 2013). MAT estimates are lower than geochemical-based SST proxies (Fig. 10; Hollis et al., 2019). Secondly, precipitation changes may have led to conditions well-suited to Casuarinaceae. Hydrogen isotopes of plant biomarkers ($\delta D_{n\text{-alkane}}$) from the Kumara-2 core (Fig. 1) show a general increase in the early Eocene, with highest values (-135‰) coeval with the *M. harrisii* increase, perhaps suggesting a more seasonal climate or increasing aridity (Handley et al., 2011). Moreover, long-term changes in temperature and precipitation patterns may have led to changes in soil conditions more favourable for Casuarinaceae. Results from the Taranaki Basin (Fig. 1) indicate enhanced chemical weathering in the early Eocene (Zone MH1), with increased quartz-K-feldspar sediments and a decline in plagioclase-rich sediments (Higgs et al., submitted).

7. Conclusions

The early Paleogene succession at mid-Waipara River, Canterbury Basin, New Zealand, has been the focus of several high-profile paleoclimate studies as the sediments contain good preservation of microfossils and organic biomarkers. Here, we build on this previous work and undertake a quantitative analysis of paleontological and multiproxy geochemical indicators of climate and environmental change through the early–middle Eocene, with particular focus on the Early Eocene Climatic Optimum (EECO).

The section spans the early Eocene (New Zealand Waipawan Stage) to middle Eocene (lower Bortonian Stage), ~55.5–42.5 Ma, with a non-exposed interval in the lower Eocene (middle Waipawan) and an unconformity, spanning ~3 Myr, in the middle Eocene (latest Heretaungan, Porangan and earliest Bortonian Stages). The EECO corresponds with a ~33.5 m interval from late Waipawan to the Mangaorapan/Heretaungan boundary, 49.27 Ma, in upper Chron C22n. The EECO onset is not captured as it occurs in the non-exposed interval, but the termination is preserved and corresponds to a sustained shift to lower TEX₈₆ values and more positive bulk carbonate $\delta^{13}\text{C}$ values. A series of six negative CIEs are identified in the EECO and tentatively correlated with named CIEs in global benthic $\delta^{13}\text{C}$ compilations. These CIEs are found to be associated with high TEX₈₆ values, indicating that they represent hyperthermals.

The TEX₈₆ record indicates that SST increased from the earliest Eocene to the early EECO, by 7°C with the TEX₈₆^H calibration and by 12°C with the BAYSPAR calibration. Peak SST for the EECO were 34°C (TEX₈₆^H calibration) and 36°C (BAYSPAR calibration). SST began to gradually decline from the middle EECO (~51 Ma) and reached minimum values for the post-EECO Heretaungan at ~47 Ma (27°C and 22°C, respectively). Similar average values are recorded for the overlying Bortonian Stage, but with significant variation in SST estimates of 6–8°C. This SST record is in good agreement with previous estimates from a lower resolution sample set using TEX₈₆ and planktic foraminiferal $\delta^{18}\text{O}$ and Mg/Ca ratios (Hollis et al., 2009, 2012; Creech et al., 2010).

We also find good agreement between the relative temperature trend for TEX₈₆ and trends in marine microfossil proxies for temperature, providing confidence that both approaches are useful guides to past water temperature. Pronounced warming in the early EECO corresponds with the most pronounced biotic changes in the section. This includes increased diversity in calcareous nannofossil and dinocyst assemblages, the highest abundance of warm-water taxa and planktic foraminifera, and a long-term shift to abundant and diverse angiosperm vegetation, primarily driven by a rise in Casuarinaceae. Marine microfossils also offer a means to evaluate the inference drawn from geochemical proxies that latitudinal temperature gradients were greatly reduced in the EECO. Our provisional analysis of microfossil assemblages indicates the latitudinal temperature gradient between

mid- and low latitudes in the EECO was greater than that indicated by geochemical SST proxies. Further biogeographic studies of microfossil assemblages are needed to determine if it is possible to quantify these gradients.

There is no clear evidence for a notable increase in sedimentation rates or accumulation of terrigenous material associated with warmest temperatures of the EECO. This contrasts with that previously documented at the nearby oceanic carbonate Mead Stream section and may reflect different sediment delivery pathways and a more dynamic coastal mid-Waipara setting. Marine surface productivity does also not appear to have increased in the warmest part of the EECO, although superabundant *Homotryblum*, a euryhaline dinocyst genus, in the early and middle EECO suggest the presence of seasonally elevated salinity levels and/or stratified surface waters. In the late EECO, from ~50 Ma, combined proxies indicate declining temperatures correspond with an increase in cool-water marine taxa and contribution of terrigenous material into the Canterbury Basin, which continued into the post-EECO.

This multi-proxy study of the continental margin mid-Waipara River section shows the value of combining well-calibrated biological and geochemical records to better constrain and understand past warm climate states, and to provide a robust means to interrogate geochemical-based temperature proxies (Hollis et al., 2019).

Acknowledgements

Roger Tremain, Henry Gard and Sonja Bermudez (GNS Science) are thanked for sample preparation. This study was supported by the New Zealand Government's Strategic Science Investment Fund through the GNS Science Global Change through Time Programme. RDP and BDAN acknowledges the ERC for funding the Advanced Grant T-GRES and the NERC for funding SWEET. BDAN acknowledges additional funding through a Royal Society Tata University Research Fellowship. We thank the two anonymous reviewers for very constructive and helpful reviews, and the editor for his comments and proofreading.

Figures

1. Location of the mid-Waipara River section in northeast South Island (A), and early Eocene (50 Ma) paleogeographic reconstruction for the Southwest Pacific based on the paleomagnetic reference frame of Matthews et al. (2016) (B). Thick red line in (A) shows the position of Ashley Mudstone samples examined in this study. HB = Hampden Beach, KC = Kumara-2 core, TB = Taranaki Basin.

2. The early and middle Eocene timescale (GTS2014, after Gradstein et al. 2012; Ogg et al., 2014; NZGTS2015, after Raine et al., 2015) and global benthic foraminiferal isotope record (Cramer et al., 2009; recalibrated to GTS2014). The age of the Mangaorapan/Heretaungan boundary is recalibrated to Westerhold et al. (2017). Ages of calcareous nannofossil (NP) zone boundaries are based on Gradstein et al. (2012), with adjustments to Zones NP9 to NP14 after Hollis et al. (2019). The New Zealand dinocyst and spore/pollen zones are from Wilson et al. (1988) and Morgans et al. (2004); *C. col* = *Charlesdowniea coleothrypta*, *C. ed* = *Charlesdowniea edwardsii*, *M. pe* = *Membranophoridium perforatum*, *W. ec* = *Wilsonidium echinosuturatum*). Grey bands represent the position of the Paleocene–Eocene Thermal Maximum (PETM) and Early Eocene Climatic Optimum (EECO).

3. Summary of the mid-Waipara River lithological column (Ashley Mudstone), and ranges of biostratigraphic marker taxa and biozones in the early to middle Eocene. Also shown are the stratigraphic distribution of samples taken from the Ashley Mudstone for both the 2007 and 2012 collections, and planktic foraminiferal abundance (%). Thickened lines indicate intervals of common (>8%) abundance. Magnetostratigraphy from Dallanave et al. (2016), NP zones are calcareous nannofossil zones.

4. Variation in calcium carbonate (CaCO₃) content (a), and calcareous nannofossil preservation (b), diversity (c) and relative abundance of biogeographic indicator taxa (d) in the mid-Waipara River section. Preservation indicators include visually observed preservation (VOP, black line and markers)

and relative abundance of *Zygrhablithus bijugatus* (red line and markers), a species sensitive to dissolution. Diversity is indicated by taxon richness (black line and markers) and the Shannon diversity index (red line and markers). Relative abundance of cool- and warm-water calcareous nannofossil groups is shown, including selected cool (*Chiasmolithus* spp. and *Reticulofenestra daviesii*) and warm-water (*Discoaster* spp., *Sphenolithus* spp., and *Coccolithus formosus*) taxa. Shaded intervals show the position of the Early Eocene Climatic Optimum (EECO, light grey) and the negative carbon isotope excursions (numbered 1 to 6, dark grey).

5. Variation in calcium carbonate (CaCO_3) content (a), bulk carbonate $\delta^{13}\text{C}$ (b), TEX_{86} (c), and BIT Index (d) for the early and middle Eocene in the mid-Waipara River section. Shaded intervals show the position of the Early Eocene Climatic Optimum (EECO, light grey) and the negative carbon isotope excursions (numbered 1 to 6, dark grey).

6. The mid-Waipara River bulk carbonate $\delta^{13}\text{C}$ and TEX_{86} records (b) compared with the benthic foraminiferal stable isotope compilation (a) for North Pacific ODP Site 1209 and South Atlantic ODP sites 1258, 1262 and 1263 of Westerhold et al. (2018), calibrated to the timescale of Westerhold et al. (2017). Grey band and dashed lines represent the Early Eocene Climatic Optimum (EECO) and carbon isotope excursions (CIEs). The six CIEs at mid-Waipara River are tentatively correlated with named CIEs as indicated.

7. The relative abundance of selected dinocyst species and genera from the early and middle Eocene in the mid-Waipara River section. Gonyaulacoid dinocysts are shown in dark grey; peridinioid dinocysts in light grey. The relative abundances of total peridinioid dinocysts and climate indicator taxa are also shown. Shaded bands represent the Early Eocene Climatic Optimum (EECO, light grey) and the negative carbon isotope excursions (dark grey).

8. The relative abundance of total terrestrial palynomorphs, selected spore and pollen species and genera, and relative proportions of spore, gymnosperm and angiosperm groups from the early and middle Eocene in the mid-Waipara River section. Shaded bands represent the Early Eocene Climatic Optimum (EECO, light grey) and the negative carbon isotope excursions (dark grey).

9. Temperature variation and associated parameters in the early and middle Eocene at mid-Waipara River section: sea surface temperature (SST) record using BAYSPAR and $\text{TEX}_{86}^{\text{H}}$ calibrations, with 95% confidence band for BAYSPAR (a), relative temperature change of SST (BAYSPAR and $\text{TEX}_{86}^{\text{H}}$) (b), and %GDGT_{RS} (c). Shaded bands represent the Early Eocene Climatic Optimum (EECO, light grey) and the negative carbon isotope excursions (dark grey).

10. Summary of available isoGDGT- and foraminifera-based SST estimates from the early and middle Eocene at mid-Waipara River, calibrated to the timescale of Westerhold et al. (2017). SSTs are derived from TEX_{86} using BAYSPAR (this study) and $\text{TEX}_{86}^{\text{H}}$ calibrations (this study and Hollis et al., 2012). Foraminifera-based SST estimates are from Mg/Ca ratios and $\delta^{18}\text{O}$ values of the mixed layer planktic genus *Morozovella* (Hollis et al., 2012, 2019). SST derived from the $\text{TEX}_{86}^{\text{H}}$ and BAYSPAR calibrations are warmer in some intervals than SST calculated from mixed layer foraminifera (Mg/Ca ratios and $\delta^{18}\text{O}$ values), and this wider variation in $\delta^{18}\text{O}$ -based SST is thought to reflect diagenetic effects (Hollis et al., 2012). Error bars are $\pm 2.5^{\circ}\text{C}$ $\text{TEX}_{86}^{\text{H}}$ and 1 sigma for Mg/Ca and $\delta^{18}\text{O}$; 95% confidence interval for BAYSPAR is shaded light blue. Shaded bands represent the Early Eocene Climatic Optimum (EECO, light grey) and negative carbon isotope excursions (dark grey).

11. The relative abundance of key calcareous nannofossil warm-water and cool-water taxa and genera from selected subtropical (Site 1210, Shatsky Rise, Northwest Pacific Ocean), temperate (Site 762, Exmouth Plateau, Indian Ocean; mid-Waipara River, Canterbury Basin; Site 277, Campbell Plateau), and polar (Site 1135, Kerguelen Plateau, Southern Indian Ocean) provinces. Data for sites 762, 1135

and 1210 are from Schneider et al. (2011). Data are recalibrated to Gradstein et al. (2012). Sites are shown on a paleogeographic reconstruction for the early Eocene, using the same reference frame as in Fig. 1 (Matthews et al., 2016). The shaded band represents the Early Eocene Climatic Optimum (EECO).

12. Summary of climate and environmental proxies for the mid-Waipara River section, plotted against age (Westerhold et al., 2017). Bulk carbonate $\delta^{13}\text{C}$ record (a), TEX_{86} -derived SST based on BAYSPAR and $\text{TEX}_{86}^{\text{H}}$ calibrations (b), % Red Sea GDGTs (c), calcareous nannofossil warm- and cool-water groups and % planktic foraminifera (d), dinocyst warm- and cooler-water groups (e), BIT index and % terrestrial palynomorphs (f), and calcareous nannofossil taxa and dinocyst peridinioids thought to be surface productivity indicators (g). Shaded bands represent the Early Eocene Climatic Optimum (EECO, light grey) and negative carbon isotope excursions (dark grey).

References

- Agnini, C., Fornaciari, E., Rio, D., Tateo, F., Backman, J., Giusberti, L., 2007. Responses of calcareous nannofossil assemblages, mineralogy and geochemistry to the environmental perturbations across the Paleocene/Eocene boundary in the Venetian Pre-Alps. *Marine Micropaleontology* 63, 19–38, doi: 10.1016/j.marmicro.2006.10.002.
- Agnini, C., Fornaciari, E., Raffi, I., Catanzariti, R., Pălike, H., Backman, J., et al., 2014. Biozonation and biochronology of Paleogene calcareous nannofossils from low and middle latitudes. *Newsletters on Stratigraphy* 47, 131–181.
- Anagnostou, E., John, E.H., Edgar, K.M., Foster, G., Ridgwell, A., Inglis, G.N., Pancost, R.D., Lunt, D.J., Pearson, P.N., 2016. Changing atmospheric CO₂ concentration was the primary driver of early Cenozoic climate. *Nature*, doi:10.1038/nature17423.
- Aubry, M.-P., 1991. Sequence stratigraphy: Eustasy or tectonic imprint? *Journal of Geophysical Research* 96, 6641–6679, doi: 10.1029/90JB01204.
- Awad, W.K., Oboh-Ikuenobe, F.E., 2016. Early Paleogene dinoflagellate cysts from ODP Hole 959D, Côte d'Ivoire-Ghana Transform Margin, West Africa: new species, biostratigraphy and paleoenvironmental implications. *Journal of African Earth Sciences* 123, 123–144.
- Backman, J., 1986. Late Paleocene to middle Eocene calcareous nannofossil biochronology from the Shatsky Rise, Walvis Ridge and Italy. *Palaeogeography, Palaeoclimatology, Palaeoecology* 57, 43–59.
- Barnet, J.S.K., Littler, K., Westerhold, T., Kroon, D., Leng, M.J., Bailey, I., Röhl, U., Zachos, J.C., 2019. A high-fidelity benthic stable isotope record of Late Cretaceous–Early Eocene climate change and carbon-cycling. *Paleoceanography and Paleoclimatology* 34, 672–679. <https://doi.org/10.1029/2019PA003556>.
- Beerling, D.J., Royer, D.L., 2011. Convergent Cenozoic CO₂ history. *Nature Geosciences* 4, 418–420.
- Bijl, P.K., Schouten, S., Sluijs, A., Reichert, G.-J., Zachos, J.C., Brinkhuis, H., 2009. Early Paleogene temperature evolution of the southwest Pacific Ocean. *Nature* 461, 776–779.
- Bijl, P.K., Pross, J., Warnaar, J., Stickley, C., Huber, M., Guerin, R., Houben, A.J.P., Sluijs, A., Visscher, H., Brinkhuis, H., 2011. Environmental forcings of Paleogene Southern Ocean dinoflagellate biostratigraphy. *Paleoceanography* 26, PA1202, doi:10.1029/2009PA001905.
- Bijl, P.K., Sluijs, A., Brinkhuis, H., 2013a. A magneto- and chemostratigraphically calibrated dinoflagellate cyst zonation of the early Paleogene South Pacific Ocean. *Earth-Science Reviews* 124, 1–31.
- Bijl, P.K., Bendle, J., Boharty, S., Pross, J., Schouten, S., Tauxe, L., Stickley, C., McKay, R., Röhl, U., Olney, M., Sluijs, A., Escutia, C., Brinkhuis, H., and Expedition 318 Scientists, 2013b. Eocene cooling linked to early flow across the Tasmanian Gateway. *Proceedings of the national Academy of Science U.S.A* 110, 9645–9650.
- Bown, P. R., 1998. *Calcareous Nannofossil Biostratigraphy*. Cambridge University. 315 p.
- Bown, P. R., 2005. Paleogene calcareous nannofossils from the Kilwa and Lind areas of coastal Tanzania (Tanzania Drilling Project 2003–4). *Journal of Nannoplankton Research* 27, 21–95.
- Bown, P. R., Young, J. R., 1998. Techniques. In Bown, P. R. (Ed.), *Calcareous Nannofossil Biostratigraphy*. London: Kluwer Academic Publishers, 16–28.
- Boudreau, B., Middelburg, J., Sluijs, A., van der Ploeg, R., 2019. Secular variations in the carbonate chemistry of the oceans over the Cenozoic. *Earth Planetary Science Letters* 512, 194–206.
- Bralower, T. J., 2002. Evidence of surface water oligotrophy during the Paleocene–Eocene thermal maximum: Nannofossil assemblage data from Ocean Drilling Program Site 690, Maud Rise, Weddell Sea. *Paleoceanography* 17, doi: 10.1029/2001pa000662.
- Brinkhuis, H., 1994. Late Eocene to Early Oligocene dinoflagellate cysts from the Priabonian type-area (northeast Italy): biostratigraphy and paleoenvironmental interpretation. *Palaeogeography, Palaeoclimatology, Palaeoecology* 107, 121–163.
- Carlson, H., Caballero, R., 2017. Atmospheric circulation and hydroclimate impacts of alternative warming scenarios for the Eocene. *Climates of the Past* 13, 1037–1048.
- Carmichael, M., Inglis, G., Badger, M., Naafs, B.D., Behrooz, L., Remmelzwaal, S., Monteiro, F., Rohrsen, M., Farnsworth, A., Buss, H., Dickson, A., Valdes, P., Lunt, D., Pancost, R.D., 2017. Hydrological and associated biogeochemical consequences of rapid global warming during the Paleocene–Eocene Thermal Maximum. *Global and Planetary Change* 157, 114–138.
- Carpenter, R.J., Jordan, G.J., Macphail, M.K., Hill, R.S., 2012. Near-tropical Early Eocene terrestrial temperatures at the Australo-Antarctic margin, western Tasmania. *Geology* 40, 267–270.
- Christophel, D.C., 1980. Occurrence of *Casuarina* megafossils in the Tertiary of South-eastern Australia. *Australian Journal of Botany* 27, 249–259.

- Contreras, L., Pross, J., Bijl, P.K., O'Hara, R.B., Raine, J.I., Sluijs, A., Brinkhuis, H., 2014: Southern high-latitude terrestrial climate change during the Paleocene–Eocene derived from a marine pollen record (ODP Site 1172, East Tasman Plateau). *Climate of the Past* 10, 1401–1420.
- Cooper, R.A. (editor), 2004. *The New Zealand Geological Timescale*. Institute of Geological and Nuclear Sciences Monograph 22. 284p.
- Cooper, T.F., 2018. Early Eocene palynology from Mead Stream, New Zealand. Master of Science (Geology) thesis, Victoria University of Wellington, December 2017.
- Cramer, B., Wright, J.D., Kent, D.V., Aubry, M.-P., 2003. Orbital climate forcing of $\delta^{13}\text{C}$ excursions in the late Paleocene–early Eocene. *Paleoceanography* 18, 1097, doi:10.1029/2003PA000909.
- Cramer, B., Toggweiler, J.R., Wright, J.D., Katz, M.E., Miller, K.G., 2009. Ocean overturning since the Late Cretaceous: Inferences from a new benthic foraminiferal isotope compilation. *Paleoceanography* 24, PA4216, doi:10.1029/2008PA001683.
- Cramwinckel, M.J., Huber, M., Kocken, I., Agnini, C., Bijl, P., Boharty, S., Frieling, J., Goldner, A., Hilgen, F., Kip, E., Peterse, F., van der Ploeg, R., Röhl, U., Schouten, S., Sluijs, A., 2018. Synchronous tropical and polar temperature evolution in the Eocene. *Nature*, doi.org/10.1038.s41586-018-0272-2.
- Creech, J.B., Baker, J., Hollis, C.J., Morgans, H.E.G., Smith, E., 2010. Eocene sea temperatures for the mid-latitude southwest Pacific from Mg/Ca ratios in planktonic and benthic foraminifera. *Earth and Planetary Science Letters* 299, 483–495.
- Crouch, E.M., Brinkhuis, H., 2005: Environmental change across the Paleocene–Eocene transition from eastern New Zealand: a marine palynological approach. *Marine Micropaleontology* 56, 138–160.
- Crouch, E.M., Heilmann-Clausen, C., Brinkhuis, H., Morgans, H., Rogers, K., Egger, H., Schmitz, B., 2001. Global dinoflagellate events associated with the late Paleocene thermal maximum. *Geology* 29, 315–318.
- Crouch, E.M., Brinkhuis, H., Visscher, H., Adatte, T., Bolle, M.-P., 2003. Late Paleocene–early Eocene dinoflagellate cyst records from the Tethys: further observations on the global distribution of *Apectodinium*. *Geological Society of America Special Paper* 369, 113–131.
- Crouch, E.M., Dickens, G.R., Brinkhuis, H., Aubry, M.-P., Hollis, C.J., Rogers, K.M., Visscher, H., 2003. The *Apectodinium* acme and terrestrial discharge during the Paleocene–Eocene thermal maximum: new palynological, geochemical and calcareous nannoplankton observations at Tawanui, New Zealand. *Palaeogeography, Palaeoclimatology, Palaeoecology* 194, 387–403.
- Dale, B., 1996. Dinoflagellate cyst ecology: modelling and geological applications. In: Jansonius, J., McGregor, D.C. (Eds.), *Palynology: Principles and Applications*. AASP Foundation, 1249–1275.
- Dallanave, E., Agnini, C., Bachtadse, V., Muttoni, G., Crampton, J.S., Strong, C.P., Hines, B.R., Hollis, C.J., Slotnick, B.S., 2015. Early to middle Eocene magneto-biochronology of the southwest Pacific Ocean and climate influence on sedimentation: Insights from the Mead Stream section, New Zealand. *Geological Society of America Bulletin* 127, 643–660.
- Dallanave, E., Bachtadse, V., Crouch, E.M., Tauxe, L., Shepherd, C.L., Morgans, H.E.G., Hollis, C.J., Hines, B.R., Sugisaki, S., 2016. Constraining early to middle Eocene climate evolution of the southwest Pacific and Southern ocean. *Earth and Planetary Science Letters* 433, 380–392.
- De Jonge, C., Hopmans, E.C., Stadnitskaia, A., Rijpstra, W.I.C., Hofland, R., Tegelaar, E., Sinninghe Damsté, J.S., 2013: Identification of novel penta- and hexamethylated branched glycerol dialkyl glycerol tetraethers in peat using HPLC–MS², GC–MS and GC–SMB–MS. *Organic Geochemistry* 54, 78–82, doi: 10.1016/j.orggeochem.2012.10.004.
- De Jonge, C., Hopmans, E.C., Zell, C.I., Kim, J.-H., Schouten, S., Sinninghe Damsté, J.S., 2014a: Occurrence and abundance of 6-methyl branched glycerol dialkyl glycerol tetraethers in soils: implications for palaeoclimate reconstruction. *Geochimica et Cosmochimica Acta* 141, 97–112, doi: 10.1016/j.gca.2014.06.013.
- De Jonge, C., Stadnitskaia, A., Hopmans, E.C., Cherkashov, G., Fedotov, A., Sinninghe Damsté, J.S., 2014b. In situ produced branched glycerol dialkyl glycerol tetraethers in suspended particulate matter from the Yenisei River, Eastern Siberia. *Geochimica et Cosmochimica Acta* 125, 476–491.
- De Vernal, A., Eynaud, F., Henry, M., Hillaire-Marcel, C., Londeix, L., Mangin, S., Matthiessen, J., Marret, F., Radi, T., Rochon, A., Solignac, S., Turon, J., 2005. Reconstruction of sea-surface conditions at middle to high latitudes of the Northern Hemisphere during the Last Glacial maximum (LGM) based on dinoflagellate cyst assemblages. *Quaternary Science Reviews* 24, 897–924.
- De Verteuil, L., Norris, G., 1996. Middle to upper Miocene *Geonettia clinae*, an opportunistic coastal embayment dinoflagellate of the *Homotryblum* complex. *Micropaleontology* 42, 263–284.
- Dickens, G.R., Castillo, M., Walker, J., 1997. A blast of gas in the latest Paleocene: simulating first-order effects of massive dissociation of oceanic methane hydrate. *Geology* 25, 259–262.

- Dunkley Jones, T., Bown, P. R., Pearson, P. N., 2009. Exceptionally well preserved upper Eocene to lower Oligocene calcareous nannofossils (Prymnesiophyceae) from the Oande Formation (Kilwa Group), Tanzania. *Journal of Systematic Paleontology* 7, 359–411.
- Dybckjær, K., 2004. Morphological and abundance variations in *Homotryblum*-cyst assemblages related to depositional environments; uppermost Oligocene–Lower Miocene, Jylland, Denmark. *Palaeogeography, Palaeoclimatology, Palaeoecology* 206, 41–58.
- Edwards, L.E., Andrele, V., 1992. Distribution of selected dinoflagellate cysts in modern marine sediments. *In*: Head, M., Wrenn, J. (eds.), *Neogene and Quaternary Dinoflagellate Cysts and Acritarchs*. American Association of Stratigraphic Palynologists, Texas, p. 250–273.
- Evans, D., Sagoo, N., Renema, W., Cotton, L., Müller, W., Todd, J., Saraswati, P.K., Stassen, P., Ziegler, M., Pearson, P., Valdes, P., Affek, H., 2018. Eocene greenhouse climate revealed by coupled clumped isotope-Mg/Ca thermometry. *Proceedings of the National Academy of Sciences*, 10.1073/pnas.1714744115.
- Frieling, J., Iakovleva, A., Reichert, G.-J., Aleksandrova, G., Gnibidenko, Z., Schouten, S., Sluijs, A., 2014. Paleocene–Eocene warming and biotic response in the epicontinental West Siberian Sea. *Geology* 42, 767–770.
- Frieling, J., Sluijs, A., 2018. Towards quantitative environmental reconstructions from ancient non-analogue microfossil assemblages: Ecological preferences of Paleocene–Eocene dinoflagellates. *Earth-Science Reviews* 185, 956–973.
- Giusberti, L., Boscolo Galazzo, F., Thomas, E., 2016. Variability in climate and productivity during the Paleocene–Eocene Thermal Maximum in the western Tethys (Forada section). *Climate of the Past* 12, 213–240.
- Gradstein, F. M., Ogg, J. G., Schmitz, M., Ogg, G., 2012. *The Geologic Time Scale 2012*. Elsevier, 1176 p.
- Greenwood, D.R., Christophel, D 2005: The origins and Tertiary history of Australian “tropical” rainforests. *In*: Bermingham, E., Dick, C., Moritz, C. (eds.), *Tropical Rainforests: past, present and future*. University of Chicago Press, p. 336–373.
- Guasti, E., Kouwenhoven, T.J., Brinkhuis, H., Speijer, R.P., 2005. Paleocene sea-level and productivity changes at the southern Tethyan margin (El Kef, Tunisia). *Marine Micropaleontology* 55, 1–17.
- Handley, L., Crouch, E.M., Pancost, R.D., 2011: A New Zealand record of sea level rise and environmental change during the Paleocene–Eocene Thermal Maximum. *Palaeogeography, Palaeoclimatology, Palaeoecology* 305, 185–200.
- Haq, B. U., 1981. Paleogene paleoceanography: early Cenozoic oceans revisited: *Oceanologica Acta* 4, supplement, 71–82.
- Haq, B. U., Premoli-Silva, I., Lohmann, G.P., 1977. Calcareous plankton paleobiosgeographic evidence for major climatic fluctuations in the early Cenozoic Atlantic Ocean. *Journal of Geophysical Research* 82, 3861–3876.
- Harris, W.K., 1965: Basal Tertiary microflora from the Princetown area, Victoria, Australia. *Palaeontographica Abt. B* 115, 75–106.
- Hayward, B.W., 1986. A guide to paleoenvironmental assessment using New Zealand Cenozoic foraminiferal faunas. *New Zealand Geological Survey Report PAL 109*. 73 p.
- Hayward, B.W., Grenfell, H., Sabaa, A.T., Neil, H., Buzas, M., 2010. Recent New Zealand deep-water benthic foraminifera: taxonomy, ecologic distribution, biogeography, and use in paleoenvironmental assessment. *GNS Science Monograph* 26. 363 p.
- Hennissen, J., Head, M., Schepper, S., Groenveld, J., 2017. Dinoflagellate cyst paleoecology during Pliocene–Pleistocene climatic transition in the North Atlantic. *Palaeogeography, Palaeoclimatology, Palaeoecology* 470, 81–108.
- Hernández-Sánchez, M.T., Woodward, E.M.S., Taylor, K.W.R., Henderson, G.M., Pancost, R.D., 2014: Variations in GDGT distributions through the water column in the South East Atlantic Ocean. *Geochimica et Cosmochimica Acta* 132, 337–348, doi: 10.1016/j.gca.2014.02.009.
- Higgs, K.E., Munday, S., Forbes, A., Crouch, E., Sagar, M., submitted. A geochemical and biostratigraphic approach to investigating regional changes in sandstone composition through the Paleocene–Eocene, Taranaki Basin, New Zealand. *Geological Magazine*.
- Hill, R.S., 1994: The history of selected Australian taxa. *In*: Hill, R.S. (ed.), *History of the Australian vegetation: Cretaceous to Recent*. Cambridge University Press, p. 390–419.
- Hines, B.R., Hollis, C.J., Atkins, C.B., Baker, J.A., Morgans, H.E.G., Strong, C.P., 2017. Reduction of oceanic temperature gradients in the early Eocene Southwest Pacific Ocean. *Palaeogeography, Palaeoclimatology, Palaeoecology* 475, 41–54.

- Holdgate, G.R., Sluiter, I.R.K., Taglieri, J., 2017: Eocene–Oligocene coals of the Gippsland and Australo-Antarctic basins - paleoclimatic and paleogeographic context and implications for earliest Cenozoic glaciations. *Palaeogeography, Palaeoclimatology, Palaeoecology* 472, 236–255.
- Hollis, C.J., 2006. Radiolarian turnover through the Paleocene–Eocene transition, Mead Stream, New Zealand. *Eclogae geol. Helv.* 99 Supplement 1, S79–S99.
- Hollis, C.J., Dickens, G.R., Field, B., Jones, C.M., Strong, C.P., 2005a. The Paleocene–Eocene transition at Mead Stream, New Zealand: a southern Pacific record of early Cenozoic global change. *Palaeogeography, Palaeoclimatology, Palaeoecology* 215, 313–343.
- Hollis, C.J., Field, B., Jones, C.M., Wilson, G.J., Dickens, G.R., 2005b. Biostratigraphy and carbon isotope stratigraphy of uppermost Cretaceous–lower Cenozoic Muzzle Group in middle Clarence valley, New Zealand. *Journal of the Royal Society of New Zealand* 35, 345–383.
- Hollis, C.J., Handley, L., Crouch, E.M., Morgans, H.E.G., Baker, J.A., Creech, J.B., Collins, K.S., Gibbs, S., Huber, M., Schouten, S., Pancost, R.D., Zachos, J.C., 2009. Tropical sea temperatures in the high-latitude South Pacific during the Eocene. *Geology* 37, 99–102.
- Hollis, C.J., Taylor, K.W.R., Handley, L., Pancost, R.D., Huber, M., Creech, J.B., Hines, B.R., Crouch, E.M., Morgans, H.E.G., Crampton, J.S., Gibbs, S., Pearson, P.N., Zachos, J.C., 2012. Early Paleogene temperature history of the Southwest Pacific Ocean: Reconciling proxies and models. *Earth and Planetary Science Letters* 349–350, 53–66.
- Hollis, C.J., Tayler, M.S., Andrew, B., Taylor, K.W., Lurcock, P., Bijl, P.B., Kulhanek, D.K., Crouch, E.M., Nelson, C.S., Pancost, R.D., Huber, M., Wilson, G.S., Ventura, G.T., Crampton, J.S., Schiøler, P., Phillips, A., 2014. Organic-rich sedimentation in the South Pacific Ocean associated with Late Paleocene climatic cooling. *Earth-Science Reviews* 134, 81–97.
- Hollis, C.J., Hines, B.R., Littler, K., Villasante-Marcos, V., Kulhanek, D.K., Strong, C.P., Zachos, J.C., Eggins, S.M., Northcote, L., Phillips, A., 2015. The Paleocene–Eocene Thermal maximum at DSDP Site 277, Campbell Plateau, southern Pacific Ocean. *Climate of the Past* 11, 1009–1025.
- Hollis, C.J., Dunkley Jones, T., Anagnostou, E., Bijl, P., Cramwinckel, M., Edgar, K., et al. 2019. The DeepMIP contribution to PMIP4: methodologies for selection, compilations and analysis of latest Paleocene and early Eocene climate proxy data. *Geoscientific Model Development*, <https://doi.org/10.5194/gmd-2018-309>.
- Hopmans, E.C., Schouten, S., Sinninghe Damsté, J.S., 2016: The effect of improved chromatography on GDGT-based palaeoproxies. *Organic Geochemistry* 93, 1–6, doi: 10.1016/j.orggeochem.2015.12.006.
- Hopmans, E.C., Weijers, J.W.H., Schefuß, E., Herfort, L., Sinninghe Damsté, J.S., Schouten, S., 2004: A novel proxy for terrestrial organic matter in sediments based on branched and isoprenoid tetraether lipids. *Earth and Planetary Science Letters* 224, 107–116.
- Huber, M., Nof, D., 2006. The ocean circulation in the southern hemisphere and its climatic impacts in the Eocene. *Palaeogeography, Palaeoclimatology, Palaeoecology* 231, 9–28.
- Huber, M., Caballero, R., 2011. The early Eocene equable climate problem revisited. *Climate of the Past* 7, 603–633.
- Huck, C.E., van de Flierdt, T., Boharty, S.M., Hammond, S.J., 2017. Antarctic climate, Southern Ocean circulation patterns, and deep water formation during the Eocene. *Palaeoceanography* 32, 674–691.
- Iakovleva, A.I., Brinkhuis, H., Cavagnetto, C., 2001. Late Paleocene–Early Eocene dinoflagellate cysts from the Turgay Strait, Kazakhstan; correlations across ancient seaways. *Palaeogeography, Palaeoclimatology, Palaeoecology* 172, 243–268.
- Iakovleva, A.I., Heilmann-Clausen, C., 2007. *Wilsonidium pechoricum* new species – a new dinoflagellate species with unusual asymmetry from the Paleocene/Eocene transition. *Journal of Paleontology* 8, 1020–1030.
- Inglis, G.N., Farnsworth, A., Lunt, D., Foster, G.L., Hollis, C.J., Pagani, M., Jardine, P.E., et al., 2015: Descent toward the Icehouse: Eocene sea surface cooling inferred from GDGT distributions. *Paleoceanography* 29 doi: 10.1002/2014PA002723.
- Jiang, S., Wise, S.W., 2009. Distinguishing the influence of diagenesis on the paleoecological reconstruction of nannoplankton across the Paleocene/Eocene Thermal Maximum: an example from the Kerguelen Plateau, southern Indian Ocean. *Marine Micropaleontology* 72, 49–59.
- Kershaw, A.P., 1970. Pollen morphological variation within the Casuarinaceae. *Pollen et Spores* 12, 145–161.
- Kim, J.-H., van der Meer, J., Schouten, S., Helmke, P., Willmott, V., Sangiorgi, F., Koç, N., et al., 2010. New indices and calibrations derived from the distribution of crenarchaeal isoprenoid tetraether lipids: Implications for past sea surface temperature reconstructions. *Geochimica et Cosmochimica Acta* 74, 4639–4654, doi: 10.1016/j.gca.2010.05.027.
- Kirtland Turner, S., Sexton, P.F., Charles, C.D., Norris, R.D., 2014. Persistence of carbon release events through the peak of early Eocene global warmth. *Nature Geoscience* 7, 748–751.

- Köthe, A., 1990. Paleogene dinoflagellates from northwest Germany: biostratigraphy and paleoenvironment. *Geol. Jahrb. A* 118, 3–111.
- Lauretano, V., Littler, K., Polling, M., Zachos, J.C., Lourens, L.J., 2015. Frequency, magnitude and character of hyperthermal events at the onset of the Early Eocene Climatic Optimum. *Climate of the Past* 11, 1313–1324.
- Lauretano, V., Hilgen, F.J., Zachos, J.C., Lourens, L.J., 2016. Astronomically tuned age model for the early Eocene carbon isotope events: A new high resolution $\delta^{13}\text{C}_{\text{benthic}}$ record of ODP Site 1263 between ~49 and ~54 Ma. *Newsletters on Stratigraphy* 49, 383–400.
- Lauretano, V., Zachos, J.C., Lourens, L.J., 2018. Orbitally paced carbon and deep-sea temperature changes at the peak of the Early Eocene Climatic Optimum. *Paleoceanography and Paleoclimatology* 33, 1050–1065, doi: 10.1029/2018PA003422.
- Littler, K., Röhl, U., Westerhold, T., Zachos, J.C., 2014. A high-resolution benthic stable-isotope record for the South Atlantic: Implications for orbital-scale changes in late Paleocene–Early Eocene climate and carbon cycling. *Earth and Planetary Science Letters* 401, 18–30.
- Lunt, D.J., Dunkley Jones, T., Heinemann, M., Huber, M., LeGrande, A., Winguth, A., Loptson, C., Marotzke, J., Roberts, C.D., Tindall, J., Valdes, P., Winguth, C., 2012. A model-data comparison for a multi-model ensemble of early Eocene atmosphere-ocean simulations: EoMIP. *Climate of the Past* 8, 1717–1736.
- Lunt, D.J., Huber, M., Anagnostou, E., Baatsen, M., Caballero, R., DeConto, R., Dijkstra, H., Donnadieu, Y., Evans, D., et al., 2017. The DeepMIP contribution to PMIP4: experimental design for model simulations of the EECO, PETM and pre-PETM (version 1.0). *Geoscientific Model Development* 10, 889–901.
- Macphail, M.K., Alley, N.F., Truswell, E.M., Sluiter, I.R.K., 1994. Early Tertiary vegetation: evidence from spores and pollen. *In: Hill, R.S. (ed.), History of the Australian vegetation: Cretaceous to Recent*. Cambridge University Press, p. 189–261.
- Martini, E., 1971. Standard Tertiary and Quaternary calcareous nannoplankton zonation. Paper presented at the Proceedings of the Second Planktonic Conference, Roma.
- Matthews, K., Maloney, K., Zahirovic, S., Williams, S., Seton, M., Müller, D., 2016. Global plate boundary evolution and kinematics since the late Paleozoic. *Global and Planetary Change* 146, 226–250.
- McGowran, B., Hill, R.S., 2015. Cenozoic climate shifts in southern Australia. *Transactions of the Royal Society of South Australia* 139, 19–37.
- McIntyre, A., Bé, A.W.H., 1967. Modern Coccolithophoridae of the Atlantic Ocean. I. Placoliths and cyrtoliths. *Deep Sea Research* 14, 561–597.
- Morgans, H.E.G., Beu, A.G., Cooper, R.A., Crouch, E.M., Hollis, C.J., Jones, C.M., Raine, J.I., Strong, C.P., Wilson, G.J., Wilson, G.S., 2004. Chapter 11, Paleogene (Dannevirke, Arnold and Landon Series). *In: Cooper, R.A. (ed.), The New Zealand Geological Timescale*. Institute of Geological and Nuclear Sciences Monograph 22, p. 125–163.
- Morgans, H.E.G., Jones, C., Crouch, E.M., Field, B.D., Raine, J.I., Strong, C.P., Wilson, G.J., 2005. Upper Cretaceous to Eocene stratigraphy and sample collections, mid-Waipara River, North Canterbury. Institute of Geological and Nuclear Sciences report 2003/08. 101p.
- Naafs, B.D.A., Pancost, R.D., 2016. Sea-surface temperature evolution across Aptian Oceanic Anoxic Event 1a. *Geology* 44, 959–962, doi: 10.1130/G38575.1.
- Naafs, B.D.A., Gallego-Sala, A.V., Inglis, G.N., Pancost, R.D., 2017a. Refining the global branched glycerol dialkyl glycerol tetraether (brGDGT) soil temperature calibration. *Organic Geochemistry* 106, 48–56, doi: 10.1016/j.orggeochem.2017.01.009.
- Naafs, B.D.A., Inglis, G.N., Zheng, Y., Amesbury, M.J., Biester, H., Bindler, R., Blewett, J., et al., 2017b. Introducing global peat-specific temperature and pH calibrations based on brGDGT bacterial lipids. *Geochimica et Cosmochimica Acta* 208, 285–301, doi: 10.1016/j.gca.2017.01.038.
- Naafs, B.D.A., Rohrsen, M., Inglis, G., Lähteenoja, O., Feakins, S., Collinson, M., Kennedy, E., Singh, P., Lunt, D., Pancost, R.D., 2018. High temperatures in the terrestrial mid-latitudes during the early Paleogene. *Nature Geoscience* 11, 766–771, doi:10.1038/s41561-018-0199-0.
- Nicolo, M.J., Dickens, G.R., Hollis, C.J., Zachos, J.C., 2007. Multiple early Eocene hyperthermals: Their sedimentary expression on the New Zealand continental margin and in the deep sea. *Geology* 35, 699–702.
- O'Brien, C., Robinson, S., Pancost, R., Sinninghe Damsté, J., Schouten, S., Lunt, D., Alsenz, H., Bornemann, A., Bottini, C., Brassell, S., Farnsworth, A., Forster, A., Huber, B., Inglis, G., Jenkyns, H., Linnert, C., Littler, K., Markwick, P., McAnena, A., Mutterlose, J., Naafs, B.D.A., Püttmann, W., Sluijs, A., van Helmond, N.A.G.M., Vellekoop, J., Wagner, T., Wrobel, N., 2017. Cretaceous sea-surface temperature evolution: Constraints from TEX₈₆ and planktonic foraminiferal oxygen isotopes. *Earth-Science Reviews* 172, 224–247, doi: 10.1016/j.earscirev.2017.07.012.
- Okado, H., Honjo, S., 1973. The distribution of oceanic coccolithophorids in the Pacific. *Deep Sea Research* 20, 355–374.

- Pälike, H., Lyle, M. (editors), 2010. Methods (Expedition 320/321 Scientists), *In* Proceedings of the Integrated Ocean Drilling Program, 320/321.
- Pancost, R.D., Taylor, K., Inglis, G.N., Kennedy, E.M., Handley, L., Hollis, C.J., Crouch, E.M., Pross, J., Huber, M., Schouten, S., Pearson, P.N., Morgans, H.E.G., Raine, J.I., 2013. Early Paleogene evolution of terrestrial climate in the SW Pacific, Southern New Zealand. *Geochemistry, Geophysics, Geosystems* 14, doi:10.1002/2013GC004935.
- Pearson, P.N., van Dongen, B., Nicholas, C.J., Pancost, R.D., Schouten, S., Singano, J., Wade, B., 2007. Stable warm tropical climate through the Eocene Epoch. *Geology* 35, 211–214.
- Perch-Nielsen, K., 1985. Cenozoic calcareous nannofossils. *In* Bolli, H., Perch-Nielsen, K., et al. (eds.), *Plankton Stratigraphy* (pp. 427–554). New York: Cambridge University Press.
- Pocknall, D.T., 1990. Palynological evidence for the early and middle Eocene vegetation and climate history of New Zealand. *Review of Palaeobotany and Palynology* 65, 57–69.
- Prasad, V., Garg, R., Khowaja-Ateequzaman, Singh, I.B., Joachimski, M., 2006. *Apectodinium* acme and palynofacies characteristics in the latest Paleocene–earliest Eocene of northeastern India: biotic response to the Paleocene–Eocene thermal maxima (PETM) in low latitude. *Journal of The Paleontological Society of India* 51, 75–91.
- Prebble, J.G., Crouch, E.M., Carter, L., Cortese, G., Bostok, H., Neil, H., 2016. An expanded modern dinoflagellate cyst dataset for the Southwest Pacific and Southern Hemisphere with environmental associations. *Marine Micropaleontology* 101, 33–48.
- Prebble, J.G., Crouch, E.M., Cortese, G., Carter, L., Neil, H., Bostok, H., 2016. Southwest Pacific sea surface conditions during Marine Isotope Stage 11 – Results from dinoflagellate cysts. *Palaeogeography, Palaeoclimatology, Palaeoecology* 446, 19–31.
- Pridier, J.N., Christophel, D.C., 2000. Distributional ecology of *Gymnostoma australianum* (Casuarinaceae), a putative palaeoendemic of Australian wet tropic forests. *Australian Journal of Botany* 48, 427–434.
- Pross, J., Schmiedl, G., 2002. Early Oligocene dinoflagellate cysts from the Upper Rhine Graben (SW Germany): paleoenvironmental and paleoclimatic implications. *Marine Micropaleontology* 45, 1–24.
- Raine, J.I., 1984. Outline of a palynological zonation of Cretaceous to Paleogene terrestrial sediments in the West Coast region, South Island. New Zealand Geological Survey report 109. 82 p.
- Raine, J.I., Kennedy, E.M., Crouch, E.M., 2009. New Zealand Paleogene vegetation and climate. *In* Crouch, E., Strong, C.P., Hollis, C. (eds.), *Climatic and Biotic Events of the Paleogene (CBEP)*, extended abstracts from an international conference in Wellington, New Zealand. GNS Science Miscellaneous Series 18, 117–122.
- Raine, J.I., Beu, A.G., Boyes, A., Campbell, H.J., Cooper, R.A., Crampton, J.S., Crundwell, M., Hollis, C.J., Morgans, H.E.G., Mortimer, N., 2015. New Zealand Geological Timescale NZGT 2015/1. *New Zealand Journal of Geology and Geophysics* 58, 398–403.
- Reay, M., 1993. Geology of the middle part of the Clarence Valley. Institute of Geological and Nuclear Sciences Geological Map 10, 1–144.
- Reichart, G.-J., Brinkhuis, H., Huiskamp, F., Zachariasse, W.J., 2004. Hyperstratification following glacial overturning events in the northern Arabian Sea. *Paleoceanography* 19, PA2013, doi:10.1029/2003PA000900.
- Schmitz, B., Pujalte, V., 2007. Abrupt increase in seasonal extreme precipitation at the Paleocene–Eocene boundary. *Geology* 35, 215–218.
- Schneider, L. J., Bralower, T. J., Kump, L. R., 2011. Response of nannoplankton to early Eocene ocean de-stratification. *Palaeoceanography, Palaeoclimatology, Palaeoecology* 310, 152–162.
- Schouten, S., Hopmans, E.C., Schefuss, E., Sinninghe Damsté, J.S., 2002. Distributional variations in marine crenarchaeotal membrane lipids: a new tool for reconstructing ancient sea water temperatures? *Earth and Planetary Science Letters* 204, 265–274, doi: 10.1016/S0012-821X(02)00979-2.
- Schouten, S., Forster, A., Panato, F., Sinninghe Damsté, J.S., 2007. Towards calibration of the TEX₈₆ palaeothermometer for tropical sea surface temperatures in ancient greenhouse worlds. *Organic Geochemistry* 38, 1537–1546, doi: 10.1016/j.orggeochem.2007.05.014.
- Shamrock, J. L., Watkins, D. K., 2012. Eocene calcareous nannofossil biostratigraphy and community structure from Exmouth Plateau, Eastern Indian Ocean (ODP Site 762). *Stratigraphy* 9, 54 pp.
- Shepherd, C. L., 2017. Early to middle Eocene calcareous nannofossils of the SW Pacific: Paleobiogeography and paleoclimate (Unpublished doctoral thesis). Victoria University of Wellington, Wellington, New Zealand. 171 p.
- Shepherd, C. L., Kulhanek, D. K., 2016. Eocene nannofossil biostratigraphy of the mid-Waipara River section, Canterbury Basin, New Zealand. *Journal of Nannoplankton Research* 36, 33–59.
- Siesser, W.G., 1993. Calcareous nannoplankton. *In* Lipps, J.H. (ed.), *Fossil Prokaryotes and Protists*. Blackwell Scientific Publications, 169–201.

- Sinninghe Damsté, J.S., Schouten, S., Hopmans, E.C., van Duin, A.C.T., Geenevasen, J., 2002. Crenarchaeol: the characteristic core glycerol dibiphytanyl glycerol tetraether membrane lipid of cosmopolitan pelagic crenarchaeota. *Journal of Lipid Research* 43, 1641–1651, doi: 10.1194/jlr.M200148-JLR200.
- Sinninghe Damsté, J.S., 2016. Spatial heterogeneity of sources of branched tetraethers in shelf systems: The geochemistry of tetraethers in the Berau River delta (Kalimantan, Indonesia). *Geochimica et Cosmochimica Acta* 186, 13–31.
- Slimani, H., Guédé, K. E., Williams, G.L., Asebriy, L., Ahmamou, M., 2016. Campanian to Eocene dinoflagellate biostratigraphy from the Tahar and Sekada sections at Arba Ayacha, western External Rif, Morocco. *Review of Palaeobotany and Palynology* 228, 26–46.
- Slotnick, B.S., Dickens, G.R., Nicolo, M.J., Hollis, C.J., Crampton, J.S., Zachos, J.C., Sluijs, A., 2012. Large-amplitude variations in carbon cycling and terrestrial weathering during the Latest Paleocene and Earliest Eocene: the record at Mead Stream, New Zealand. *The Journal of Geology* 120, 487–505.
- Slotnick, B.S., Dickens, G.R., Hollis, C.J., Crampton, J.S., Strong, C.P., Phillips, A., 2015. The onset of the Early Eocene Climatic Optimum at Branch Stream, Clarence River valley, New Zealand. *New Zealand Journal of Geology and Geophysics* 58, 262–280.
- Sluijs, A., Pross, J., Brinkhuis, H., 2005. From greenhouse to icehouse; organic-walled dinoflagellate cysts as paleoenvironmental indicators in the Paleogene. *Earth-Science Reviews* 68, 281–315.
- Sluijs, A., Brinkhuis, H., 2009. A dynamic climate and ecosystem state during the Paleocene–Eocene Thermal Maximum: inferences from dinoflagellate cyst assemblages on the New Jersey Shelf. *Biogeosciences* 6, 1755–1781.
- Steane, D.A., Wilson, K.L., Hill, R.S., 2003. Using *matK* sequence data to unravel the phylogeny of Casuarinaceae. *Molecular Phylogenetics and Evolution* 28, 47–59.
- Taylor, K.W.R., Huber, M., Hollis, C.J., Hernandez-Sanchez, M.T., Pancost, R.D., 2013. Re-evaluating modern and Palaeogene GDGT distributions: Implications for SST reconstructions. *Global and Planetary Change* 108, 158–174, doi: 10.1016/j.gloplacha.2013.06.011.
- Taylor, K.W.R., Willumsen, P.S., Hollis, C.J., Pancost, R.D., 2018. South pacific evidence for the long-term climate impact of the Cretaceous/Paleogene boundary event. *Earth-Science Reviews* 179, 287–302.
- Tierney, J.E., Tingley, M.P., 2014. A Bayesian, spatially-varying calibration model for the TEX₈₆ proxy. *Geochimica et Cosmochimica Acta* 127, 83–106, doi: 10.1016/j.gca.2013.11.026.
- Tierney, J.E., Tingley, M.P., 2015. A TEX₈₆ surface sediment database and extended Bayesian calibration. *Scientific Data* 2, 150029, doi: 10.1038/sdata.2015.29.
- Tierney, J.E., Sinninghe Damsté J., S., Pancost, R.D., Sluijs, A., Zachos, J.C., 2017. Eocene temperature gradients. *Nature Geoscience* 10, 538–539.
- Trommer, G., Siccha, M., van der Meer, M.T.J., Schouten, S., Sinninghe Damsté, J.S., Schulz, H., Hemleben, C., et al., 2009. Distribution of Crenarchaeota tetraether membrane lipids in surface sediments from the Red Sea. *Organic Geochemistry* 40, 724–731, doi: 10.1016/j.orggeochem.2009.03.001.
- Van Hinsbergen, D., de Groot, L., van Schaik, J., Spakman, W., Bijl, P., Sluijs, A., Langereis, C., Brinkhuis, H., 2015. A Paleolatitude Calculator for Paleoclimate Studies, *PLOS ONE*, 10, 10.1371/journal.pone.0126946.
- Villa, G., Persico, D., 2006. Late Oligocene climatic changes: Evidence from calcareous nannofossils at Kerguelen Plateau Site 748 (Southern Ocean). *Palaeogeography, Palaeoclimatology, Palaeoecology* 231, 110–119, doi: 10.1016/j.palaeo.2005.07.028.
- Villa, G., Fioroni, C., Pea, L., Bohaty, S., Persico, D., 2008. Middle Eocene–late Oligocene climate variability: Calcareous nannofossil response at Kerguelen Plateau, Site 748. *Marine Micropaleontology* 69, 173–192, doi: 10.1016/j.marmicro.2008.07.006.
- Wei, W., Wise, S. W., 1990. Biogeographic gradients of middle Eocene–Oligocene calcareous nannoplankton in the South Atlantic Ocean. *Palaeogeography, Palaeoclimatology, Palaeoecology* 79, 29–61, doi: 10.1016/0031-0182(90)90104-F.
- Weijers, J.W.H., Schouten, S., Hopmans, E.C., Geenevasen, J.A.J., David, O.R.P., Coleman, J.M., Pancost, R.D., et al., 2006. Membrane lipids of mesophilic anaerobic bacteria thriving in peats have typical archaeal traits. *Environmental Microbiology* 8, 648–657, doi: 10.1111/j.1462-2920.2005.00941.x.
- Weijers, J.W.H., Schouten, S., van den Donker, J.C., Hopmans, E.C., Sinninghe Damsté, J.S., 2007. Environmental controls on bacterial tetraether membrane lipid distribution in soils. *Geochimica et Cosmochimica Acta* 71, 703–713, doi: 10.1016/j.gca.2006.10.003.
- Westerhold, T., Röhl, U., 2009. High resolution cyclostratigraphy of the early Eocene – new insights into the origin of the Cenozoic cooling trend. *Climate of the Past* 5, 309–327.
- Westerhold, T., Röhl, U., Laskar, J., 2012. Time scale controversy: Accurate orbital calibration of the early Paleogene. *Geochimica, Geophysics, Geosystems* 13, Q06015, doi:10.1029/2012GC004096.

- Westerhold, T., Röhl, U., Frederichs, T., Agnini, C., Raffi, I., Zachos, J.C., Wilkins, R.H., 2017. Astronomical calibration of the Ypresian Time Scale: Implications for seafloor spreading rates and the chaotic behaviour of the solar system? *Climate of the Past* 13, 1129–1152.
- Westerhold, T., Röhl, U., Donner, B., Zachos, J.C., 2018. Global extent of the Early Eocene hyperthermal events – a new Pacific benthic foraminiferal isotope record from Shatsky Rise (ODP site 1209). *Paleoceanography and Paleoclimatology* 33, 626–642, doi:10.1029/2017PA003306.
- Wilson, G.J., 1984. New Zealand Late Jurassic to Eocene dinoflagellate biostratigraphy – a summary. *Newsletters on Stratigraphy* 13, 104–117.
- Wilson, G.J., 1988. Paleocene and Eocene dinoflagellate cysts from Waipawa, Hawkes Bay, New Zealand. *New Zealand Geological Survey Paleontological Bulletin* 57, 96p.
- Wrenn, J.H., Beckman, S.W., 1982. Maceral, total organic carbon and palynological analyses of Ross Ice Shelf Project Site J9 cores. *Science* 216, 187–189, doi:10.1126/science.216.4542.187.
- Zachos, J.C., Pagani, M., Sloan, L., Thomas, E., Billups, K., 2001. Trends, rhythms, and aberrations in global climate 65 Ma to present. *Science* 292, 686–693.
- Zachos, J.C., Schouten, S., Bohart, S., Quattlebaum, T., Sluijs, A., Brinkhuis, H., Gibbs, S., Bralower, T., 2006. Extreme warming of mid-latitude coastal ocean during the Paleocene–Eocene Thermal Maximum: Inferences from TEX86 and isotope data. *Geology* 34, 737–740.
- Zachos, J.C., Dickens, G.R., Zeebe, R.E., 2008. An early Cenozoic perspective on greenhouse warming and carbon-cycle dynamics. *Nature* 45, 279–283.
- Zhang, Y.G., Zhang, C.L., Liu, X.-L., Li, L., Hinrichs, K., Noakes, J.E., 2011. Methane Index: A tetraether archaeal lipid biomarker indicator for detecting the instability of marine gas hydrates. *Earth and Planetary Science Letters* 307, 525–534.
- Zonneveld, K.A.F., Marret, F., Versteegh, G., Bogus, K., Bonnet, S., Bouimetarhan, I., Crouch, E.M., de Vernal, A., et al., 2013. Atlas of modern dinoflagellate cyst distribution based on 2045 data points. *Review of Palaeobotany and Palynology* 191, 1–197.

Figure 1

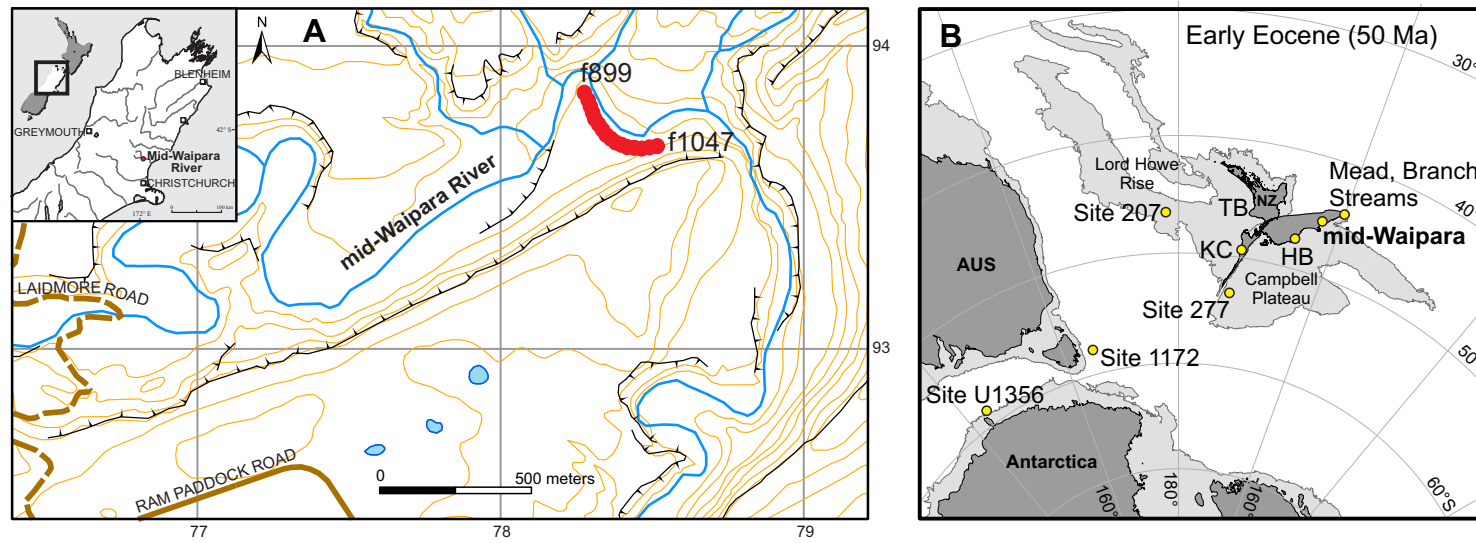


Figure 2

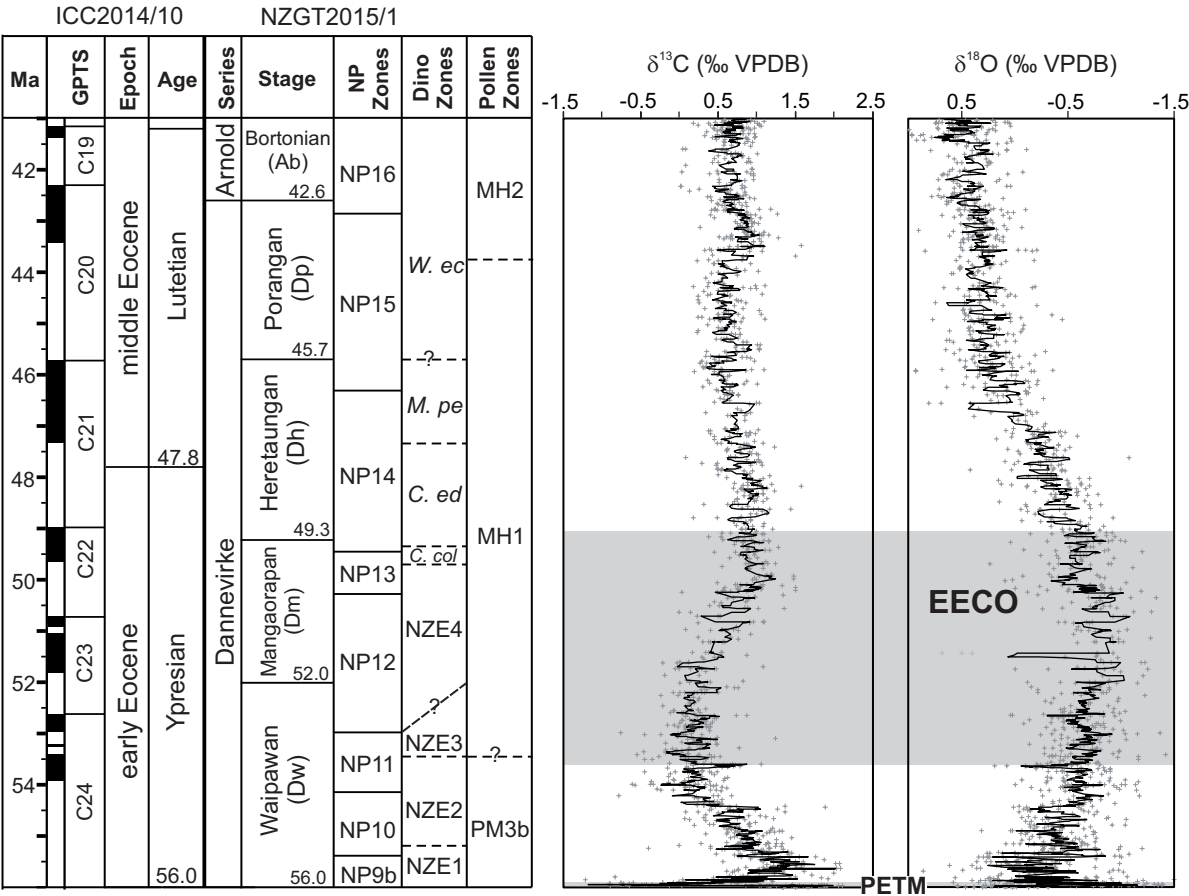


Figure 3

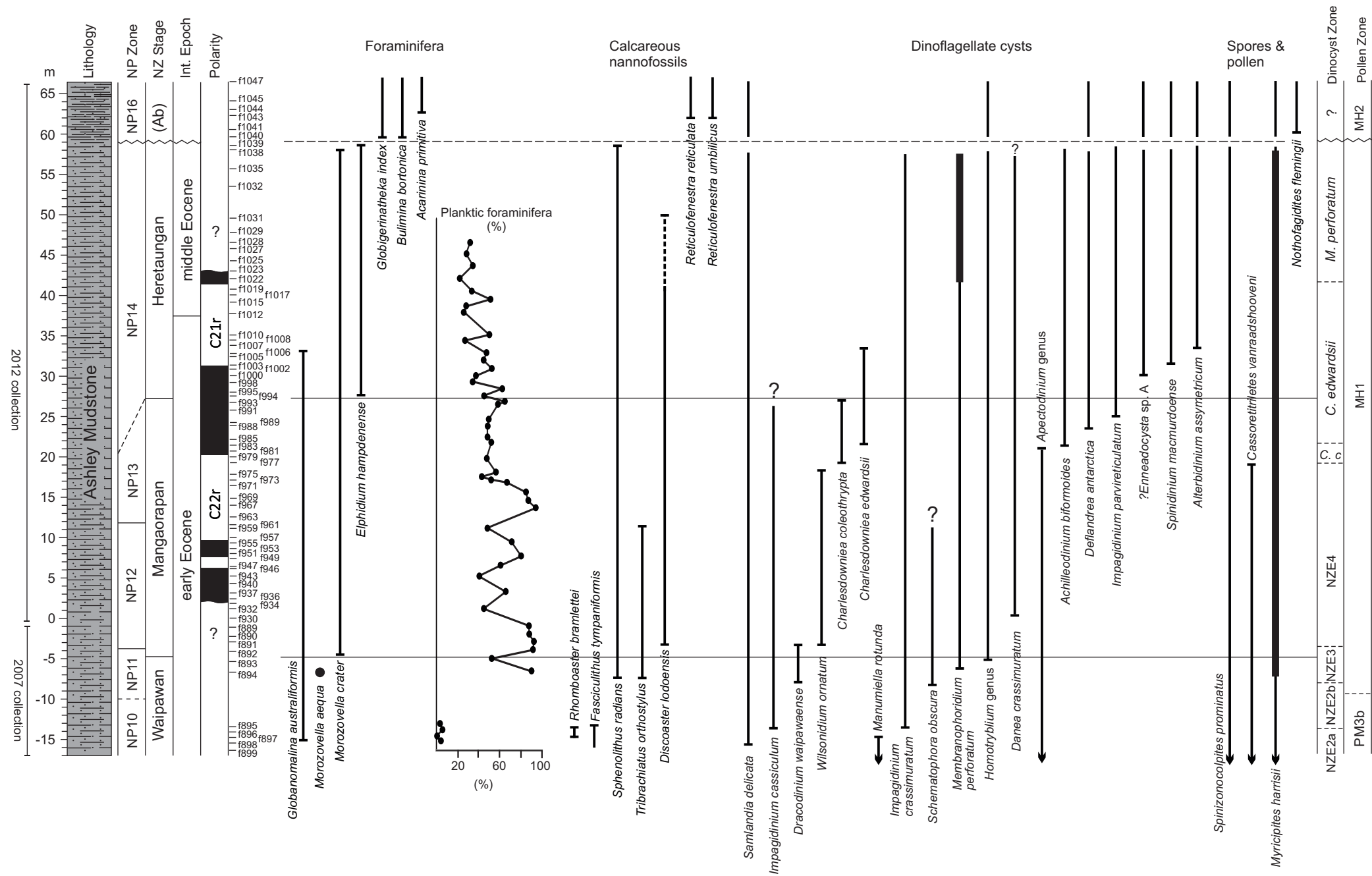


Figure 4

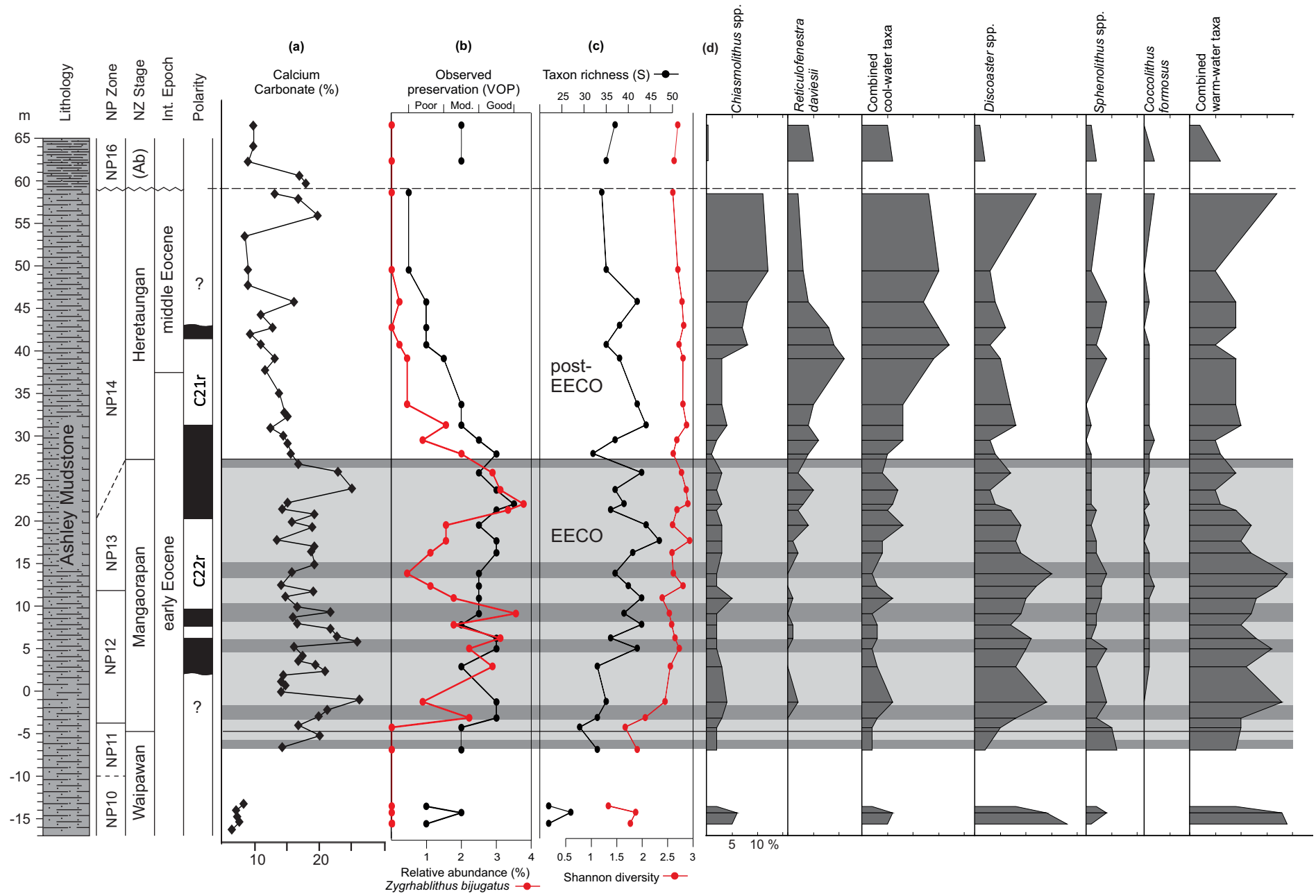


Figure 5

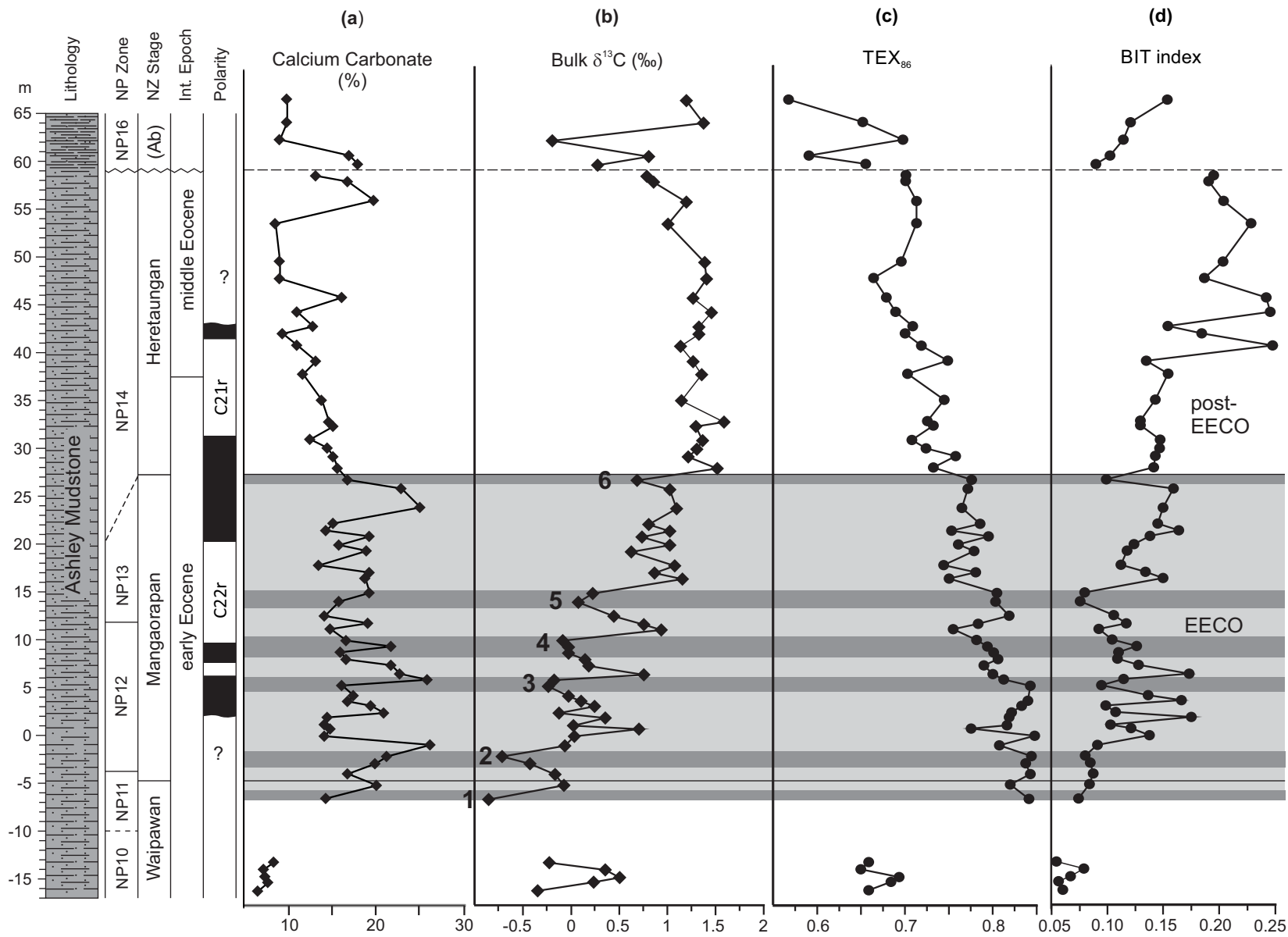


Figure 6

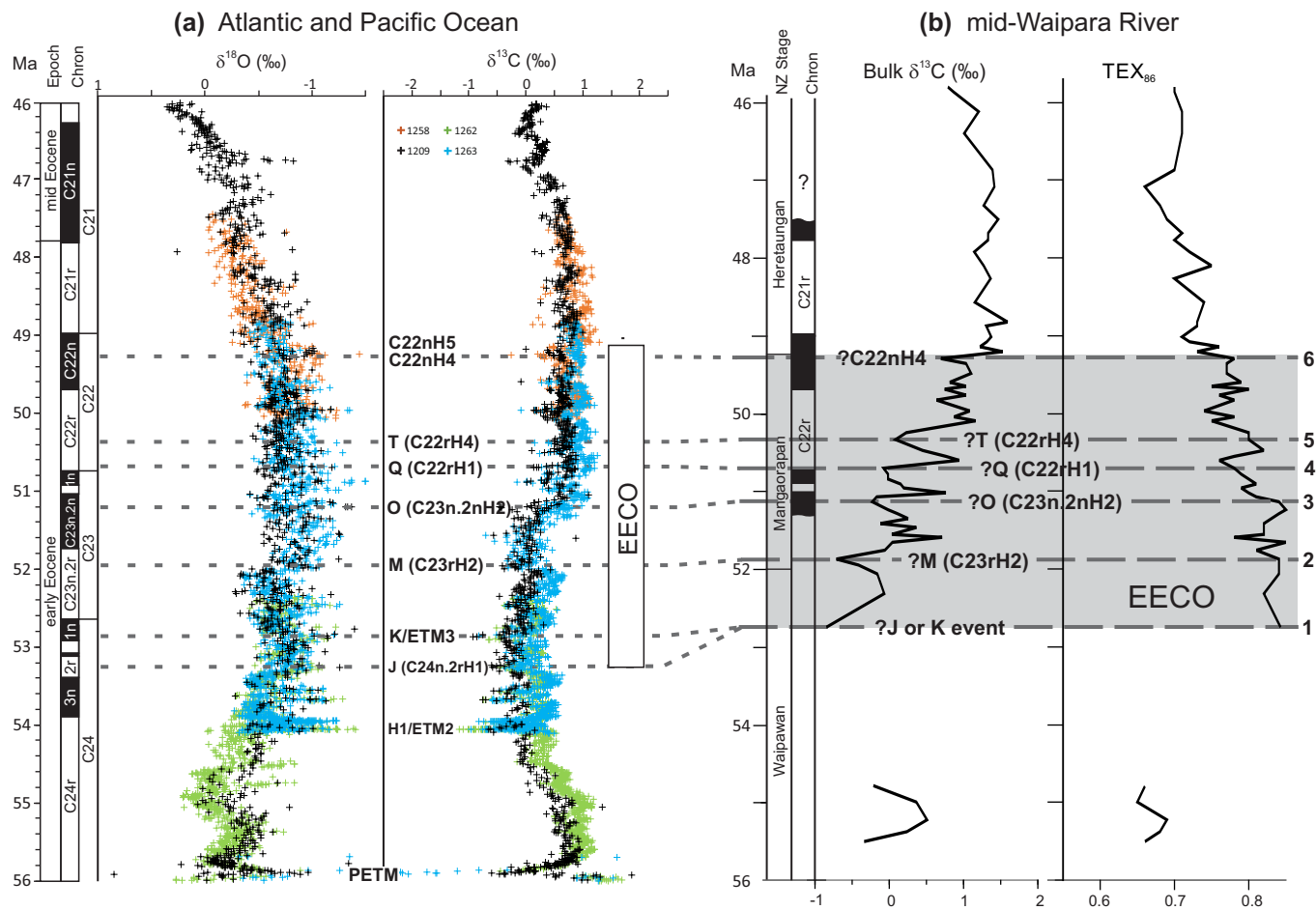


Figure 7

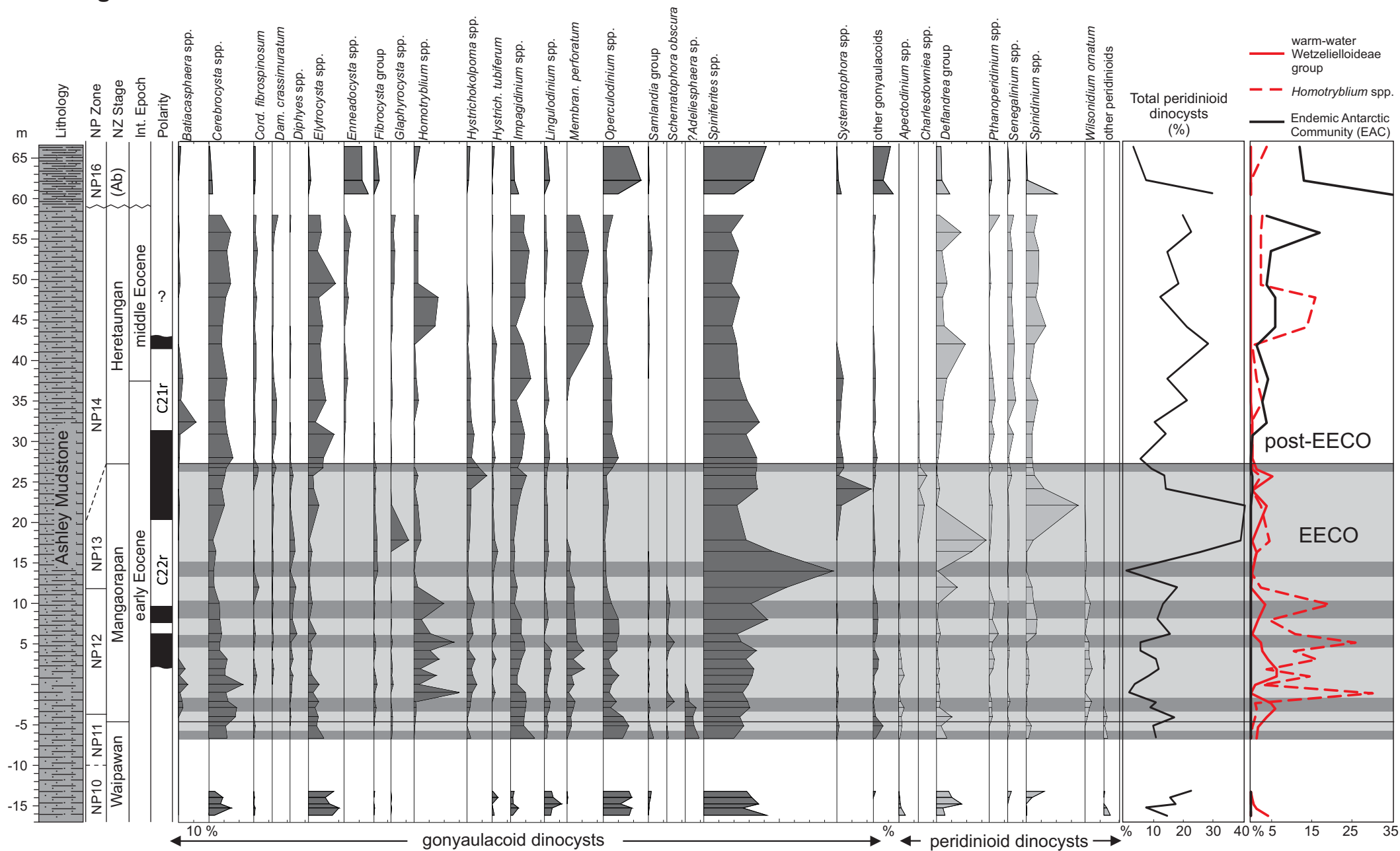


Figure 8

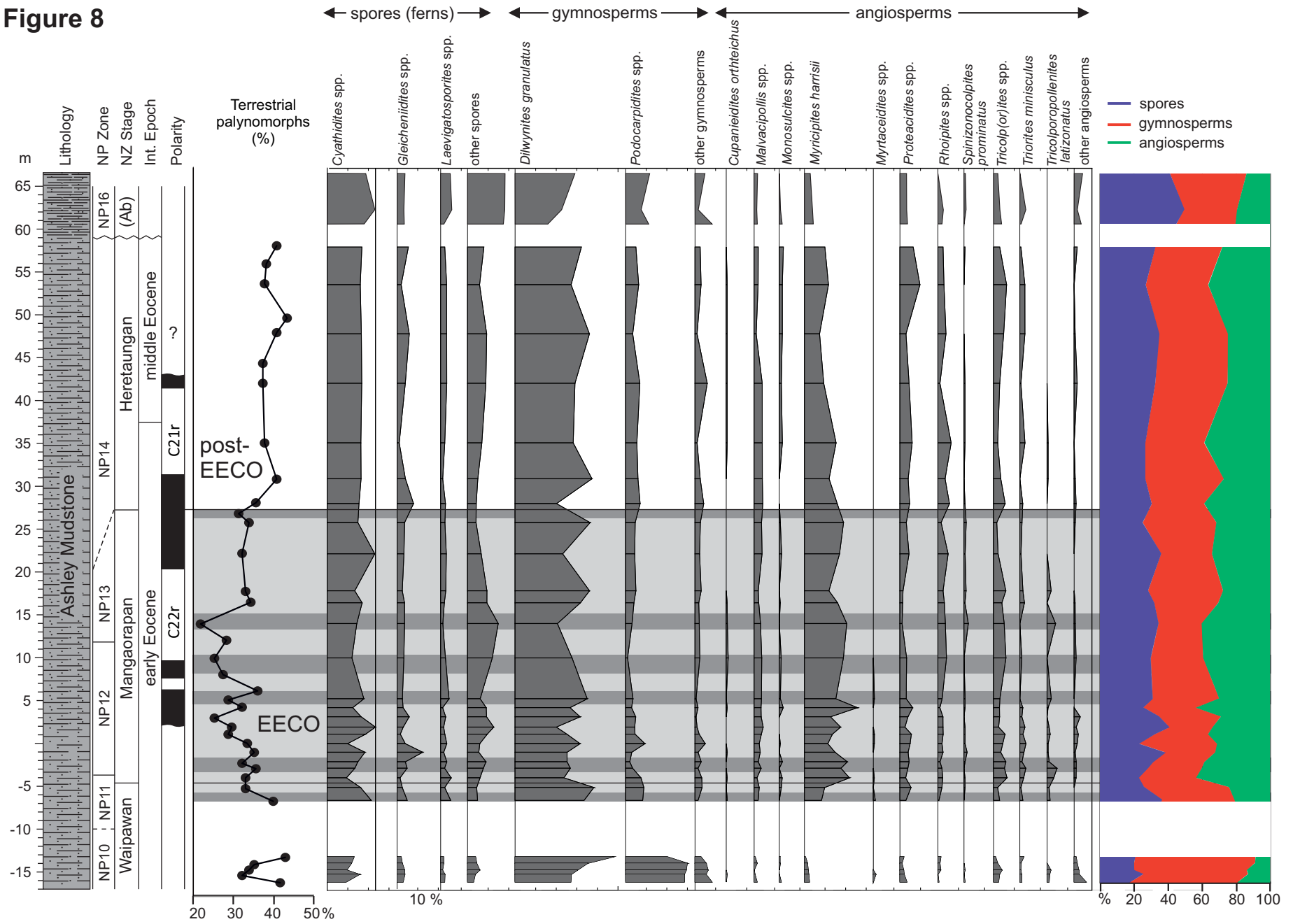


Figure 9

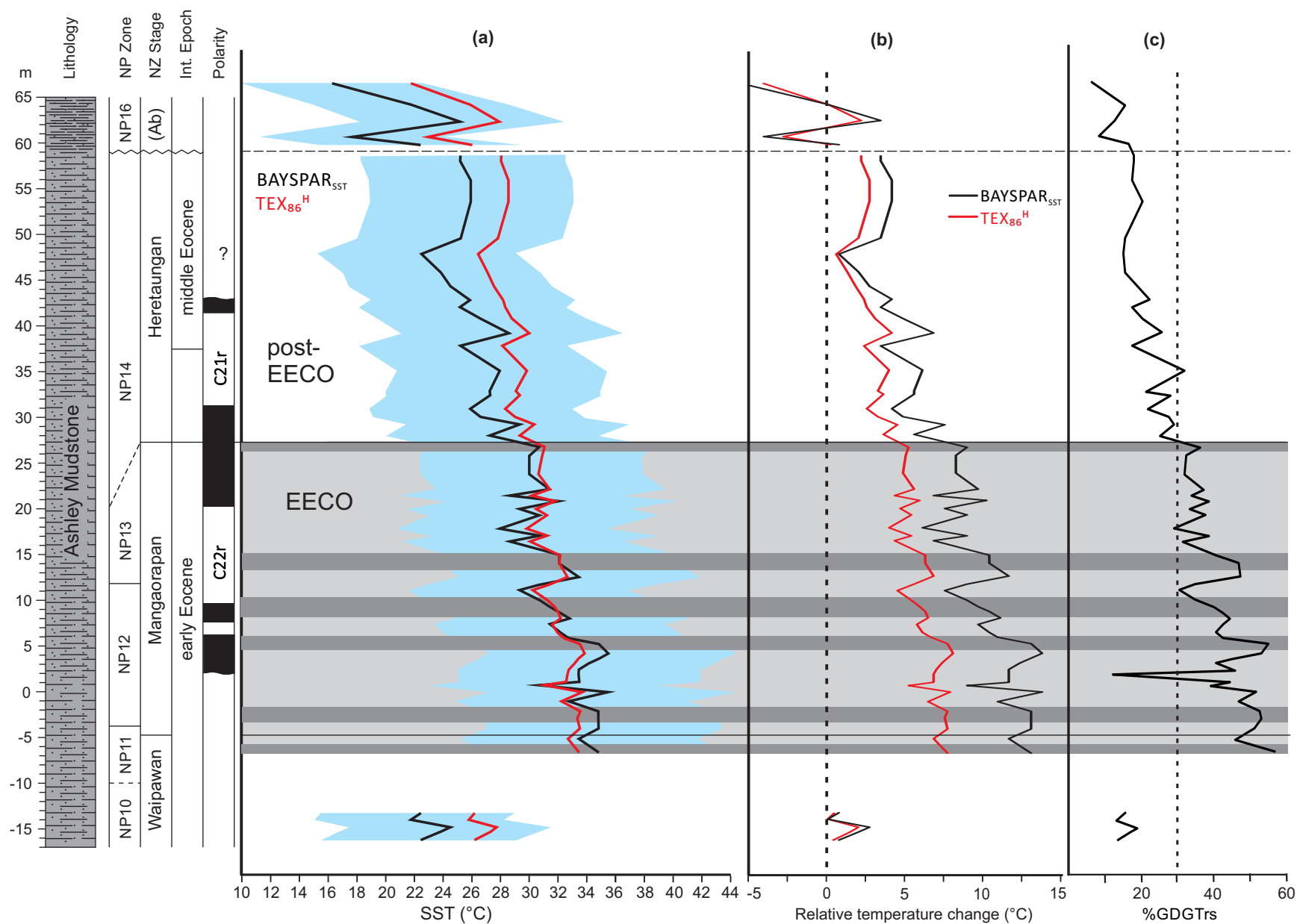


Figure 10

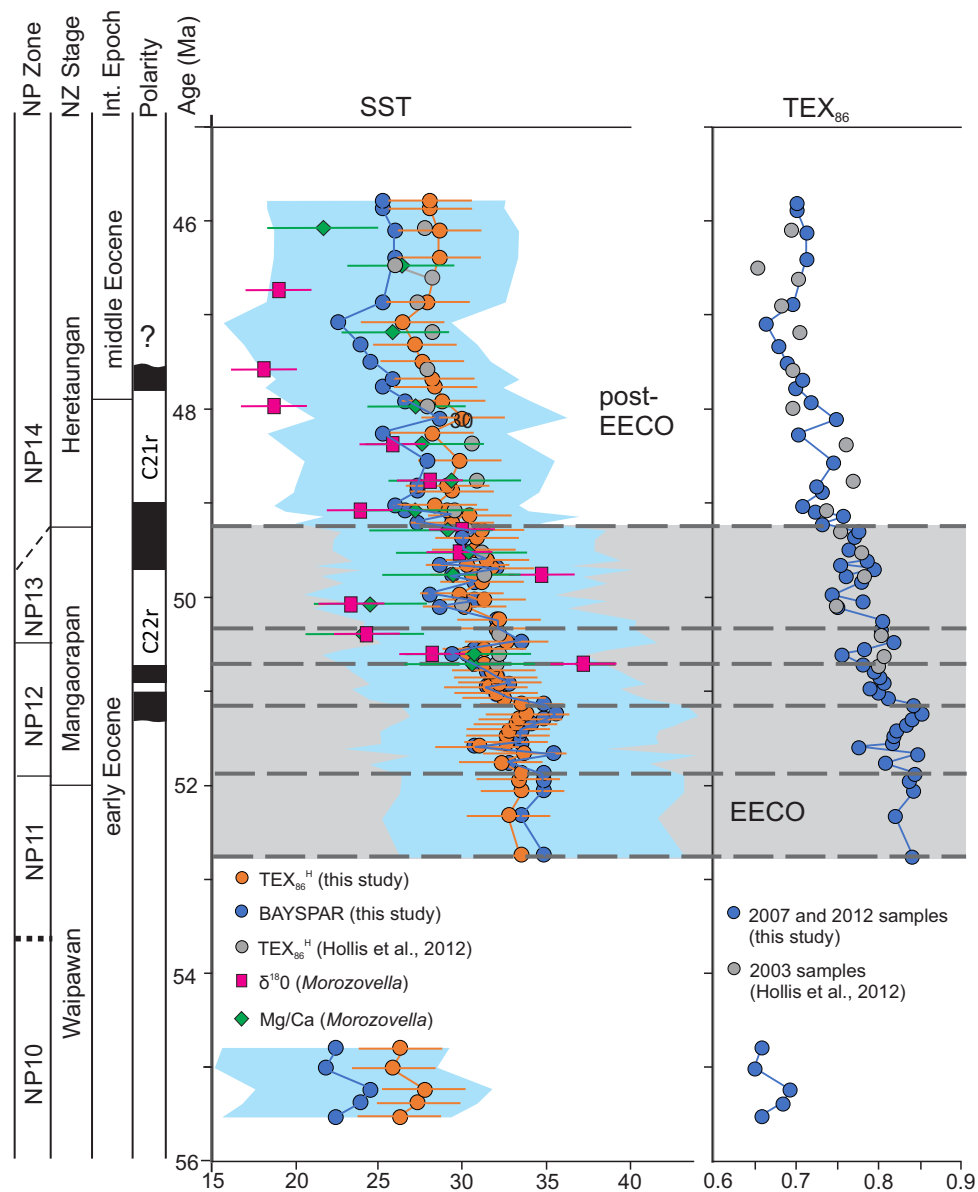


Figure 11

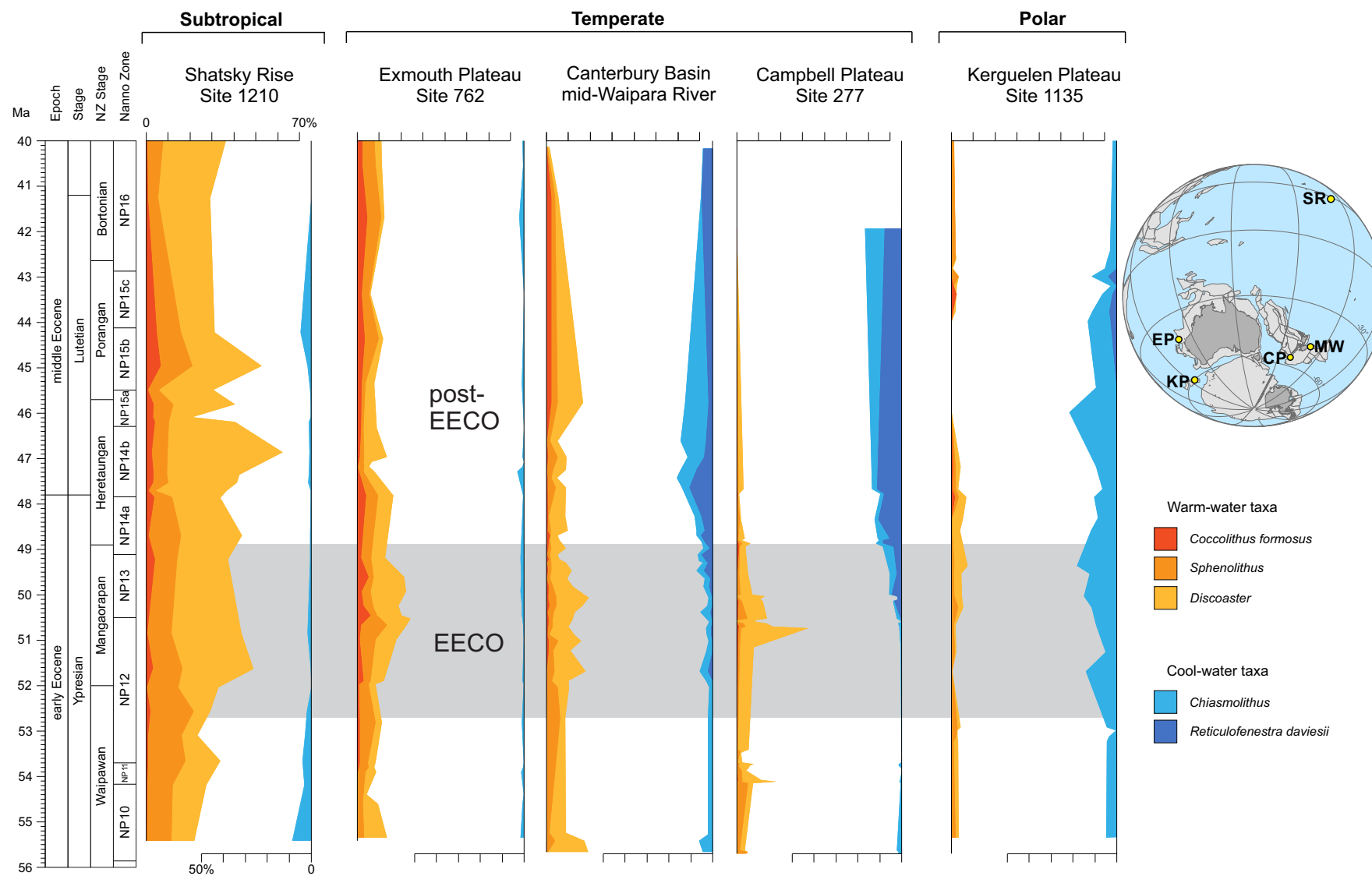


Figure 12

